https://doi.org/10.5194/egusphere-2026-2656
Preprint. Discussion started: 29 May 2026

A satellite-observed climatology of global temporal autocorrelations can be related to aerosol lifetimes.

Nick Schutgens [1], Elisabeth J. Andrews [2,3], Antti Arola [4], Yusuf Bhatti [5], Guangliang Fu[5], Otto Hasekamp [5], Pekka Kolmonen [4], Antti Lipponen [4], Tero Mielonen [4], Leighton Reygare [6,7,8], and Andrew M. Sayer [9,10]

[1]Vrije Universiteit, 1081 HV Amsterdam, the Netherlands
[2]CIRES, University of Colorado, Boulder CO 80309 USA
[3]NOAA/Global Monitoring Laboratory, Boulder CO 80305 USA
[4]FMI, P.O. Box 1627, FI-70211 Kuopio, Finland
[5]SRON Space Research Organisation Netherlands, 2333 CA Leiden, the Netherlands
[6]Met Office Hadley Centre, Exeter, UK
[7]School of Earth and Environment, University of Leeds, University of Leeds, Leeds, UK
[8]Centre for Environmental Modelling and Computation, University of Leeds, Leeds, UK
[9]Goddard Earth Sciences Technology And Research (GESTAR) II, University of Maryland, Baltimore, MD, USA
[10]NASA Goddard Space Flight Center, Greenbelt, MD 20771 USA

Correspondence: Nick Schutgens (n.a.j.schutgens@vu.nl)

Abstract. Temporal autocorrelations of aerosol are often reported, but poorly understood. We use simple box models, Perturbed Parameters Ensembles of global aerosol models, AEROCOM (AEROsol Comparison of Observations and Models) simulations as well as satellite and AERONET (AErosol RObotic NETwork) observations to study temporal autocorrelations in aerosol optical depth (AOD). In particular, we present the first global climatology of observed temporal autocorrelations.

We develop a conceptual model for autocorrelations and relate them to important timescales, in particular lifetimes. We identify aerosol processes that affect autocorrelations and find autocorrelations provide information independent from yearly AOD, in particular on deposition processes. It is possible to estimate temporal autocorrelations in AOD from satellite observations by sensors like MODIS (MODerate resolution Imaging Spectroradiometer) or POLDER (POLarization and Directionality of the Earth's Reflectances).

In our unique global climatology of observed temporal autocorrelations, regional variation is significant. Over remote oceans, the autocorrelation after 6 days tends to be low (~ 0.2 or lower) but it is quite high in tropical outflow regions (~ 0.5). Over land, it varies considerably, from 0.2 to 0.7. These spatial variations are much larger than observed year-to-year variation.

AEROCOM models often significantly overestimate autocorrelations. This suggests that loss processes are underestimated and/or contributions from seasonal sources are overestimated, which should have a marked impact on aerosol forcing estimates.

Autocorrelations offer a new way to understand aerosol processes and evaluate models. Autocorrelations can be derived from existing observational datasets, for example surface black carbon mass concentrations or cloud condensation nuclei.

https://doi.org/10.5194/egusphere-2026-2656
Preprint. Discussion started: 29 May 2026

1 Introduction

Aerosol is an important component of the Earth's atmosphere that affects the planet's climate, the biosphere, and human health. Aerosol particles scatter and absorb sunlight as well as modify clouds. Anthropogenic aerosol changes the radiative balance and influences climate change (Angstrom, 1962; Twomey, 1974; Albrecht, 1989; Hansen et al., 1997; Lohmann and Feichter, 1997, 2005). It may negatively affect solar power generation (Li et al., 2017; Labordena et al., 2018). Soluble iron, phosphate and nitrate can be transported as aerosol over long distances and provide nutrients for the biosphere (Swap et al., 1992; Vink and Measures, 2001; McTainsh and Strong, 2007; Maher et al., 2010; Émeline Lequy et al., 2012). Aerosol can penetrate deep into lungs and may carry toxins or serve as disease vectors (Dockery et al., 1993; Brunekreef and Holgate, 2002; Ezzati et al., 2002; Smith et al., 2009; Beelen et al., 2013; Ballester et al., 2013).

Annual global mean Aerosol Optical Depth (AOD) is often analysed from the following equation

$$\text{AOD} = E \times T \times \text{MEC}, \tag{1}$$

where E are the emissions, T the lifetime and MEC the Mass Extinction Coefficient (MEC, here, is a column-average and depends on wavelength, in this paper we will use 550 nm). The aerosol column burdens are $B = E \times T$. Textor et al. (2007) showed that diversity in burdens across Phase I AEROCOM[1] models was as much due to diversity in emissions as in lifetimes, with the exception of sea-salt where emissions seemed to matter more. Gliß et al. (2021) analysed Phase III AEROCOM models and showed that lifetime was actually a larger contributor to diversity in burdens than emissions for black carbon, dust and sea-salt but not for NO_3 or organic aerosol.

While extensive work has been done on creating emission inventories using either bottom-up or top-down approaches, and reducing their uncertainties, much less effort has been spent on evaluating lifetimes. Part of the explanation is that lifetimes are an emergent property of models, resulting from a variety of interacting processes while inventories are boundary conditions that are enforced on a model.

Lifetimes are time-scales that teach us something about the persistence of aerosol, but they are not readily observable. Presumably the most practical way would be to obtain estimates of yearly emissions and burdens and calculate $T = B/E$. While emission inventories exist, no observational estimates of burdens are available. Decorrelation times are however observable and, just like lifetimes, indicative of the persistence of aerosol. One can wonder if there is a connection between lifetimes and decorrelation times.

Decorrelation times can be derived from temporal autocorrelations. Given an infinite time-series $f(t)$, we can calculate the temporal autocorrelation, also known as lagged correlation, at lag τ as (Press et al., 1989):

$$\rho(\tau) = \frac{< (f(t) - \mu))\,(f(t+\tau) - \mu) >}{\sigma^2}, \tag{2}$$

where $<>$ indicates a time average, with mean $\mu =< f(t) >$ and variance $\sigma^2 =< (f(t) - \mu)^2 >$, see Sect. 2.6 for the expression in case of a finite, discrete time-series for real observations. One can speak of the correlation at a certain lag τ, e.g. ρ_6

[1] https://aerocom.met.no

https://doi.org/10.5194/egusphere-2026-2656
Preprint. Discussion started: 29 May 2026

which is the correlation at a lag of six days and will feature heavily in this study. We can also define the decorrelation time τ^* as given by the e-folding time:

$$\rho(\tau^*) = e^{-1} \tag{3}$$

Decorrelation times have been used to study persistence (Benkovitz et al., 1994; Nowosad et al., 2015; Schepanski et al., 2015; Perkins et al., 2022) or periodicities (Wehner and Wiedensohler, 2003) of aerosol. Decorrelation times have also been used to assess the representativity of observations (Masonis et al., 2002; Anderson et al., 2003; Asmi et al., 2011; Schepanski et al., 2015; Andrews et al., 2017; Kaku et al., 2018; Sayer, 2020; Chau et al., 2021).

Benkovitz et al. (1994) calculated decorrelation times of about 10 hours for modelled sulphate columns over the North Atlantic. Masonis et al. (2002) estimated decorrelation times for various optical properties (e.g. extinction, absorption, and back-scatter ratio) for in-situ campaign data and obtained values from less than an hour to 2 days. Anderson et al. (2003) found decorrelation times of 30 to 700 hours for surface extinction measurements. Wehner and Wiedensohler (2003), studying submicrometer urban aerosol number concentrations in Leipzig (Germany), found decorrelation times from a few hours to less than a day, with larger particles showing longer decorrelation times. Asmi et al. (2011) considered the autocorrelation after 1 hour of surface Cloud Condensation Nuclei (CCN) measurements for sites in Europe and found very high autocorrelations ($\geq 0.94 - 0.98$) for larger particles (diameters ≥ 100 nm) and somewhat smaller autocorrelations ($\geq 0.82 - 0.93$) for smaller particles (diameters between 30 and 50 nm). Schepanski et al. (2015) estimated temporal correlation lengths of 118 to 240 hours for Mediteranean AERONET[2] sites during dust episodes. Nowosad et al. (2015) found decorrelation times for pollen in several Polish cities from 3 to 10 days. Andrews et al. (2017) found decorrelation times from 6 to more than 24 hours for AOD and AAOD (absorption AOD) from AERONET. Kaku et al. (2018) found temporal decorrelation times of 3 days for surface $PM_{2.5}$ measurements but only a day for AOD observations. Sayer (2020) calculated decorrelation times (there defined as $\rho(\tau^*) = e^{-3}$) of a few days for AERONET sites, with tropical biomass burning sites showing longer decorrelation times of about a week. Perkins et al. (2022) found very short temporal decorrelation times of a few hours for CCN (3 hrs at 10% super saturation (SS) and 8 hours at 1% SS) at the US Southern Great Plains site. Chau et al. (2021) obtained decorrelation times of 1 day to 2 weeks for surface $PM_{2.5}$ but 1 to 3 days for satellite AOD for several cities in the Middle East.

In addition to temporal autocorrelations, there are also spatial autocorrelations that have been studied for aerosol (Targino et al., 2005; Kovacs, 2006; Afonin et al., 2008; Shinozuka and Redemann, 2011; Weigum et al., 2012; Nowosad et al., 2015; Mishra et al., 2016; Sullivan et al., 2017; Chau et al., 2021; Leblanc et al., 2022) but they are not part of this paper.

In spite of the many studies of temporal autocorrelations, no global dataset of autocorrelations exists. We also have neither a conceptual nor a process-based understanding of what determines temporal autocorrelations.

In this paper, we will provide, for the first time, a global climatology of satellite-observed autocorrelations. In addition, we will address the following questions: how are temporal autocorrelations (and in particular decorrelation times) related to lifetimes? Which aerosol processes affect temporal autocorrelations? Is it possible to observe temporal autocorrelations

[2]AErosol RObotic NETwork, `https://aeronet.gsfc.nasa.gov`

https://doi.org/10.5194/egusphere-2026-2656
Preprint. Discussion started: 29 May 2026

from Low-Earth-Orbit (LEO) satellites (to leverage their global coverage)? How do AEROCOM models evaluate against observations of autocorrelations?

The paper is structured as follows. Section 2 describes the observational and model datasets we'll use, as well as the collocation procedure for creating subsets of the data with identical spatio-temporal sampling. It also provides the definition of temporal autocorrelation and how we adapt this into an algorithm that can deal with spatio-temporally sparse data. Section 3 provides a conceptual model of temporal autocorrelations using a simple box model, while Sect. 4 explores which aerosol processes determine autocorrelations using Perturbed Parameter Ensembles (PPEs). The evaluation of satellite-observed autocorrelations with AERONET is shown in Sect. 5. A comparison of autocorrelations in various satellite products is given in Sect. 6. A global climatology of temporal autocorrelations is shown in Sect. 7, together with an analysis of interannual variability. An evaluation of AEROCOM[3] model autocorrelations is shown in Sect. 8. The paper ends with a summary and discussion in Conclusions. This paper comes with supplementary material to which we often refer for additional support of our work.

2 Observations, models and methods

2.1 AERONET

AERONET (Holben et al., 1998) Direct Sun L2.0 V3 (Giles et al., 2019; Smirnov et al., 2000) data were downloaded from `https://aeronet.gsfc.nasa.gov`. The main product is AOD at 550nm, which was interpolated from nearby wavelengths. These AOD observations are based on direct transmission measurements of solar light and have a high accuracy of ± 0.01 (Eck et al., 1999; Schmid et al., 1999). Only sites that were identified as having a high degree of maintenance ($q \geq 2$) by Kinne et al. (2013) were used. Mountain sites (altitude ≥ 1500 m) were also removed, as well as four sites (Canberra, Crozet Island, Amsterdam Island and Tinga Tingana) that have low correlations with and/or high biases vs *all* satellite products (Schutgens et al., 2020). The final AERONET data used in the current study is identical to that used in Schutgens et al. (2020).

2.2 Satellite products

As part of the AEROCOM Remote Sensing experiment, original satellite L2 data were aggregated unto a regular spatio-temporal grid with spatio-temporal grid-boxes of $1^o \times 1^o \times 30^{\min}$. These super-observations are more representative of global model grid-boxes ($\sim 1^o - 3^o$ in size) while allowing accurate temporal collocation with other datasets. The use of super-observations also reduces data amount significantly without much loss of information (at the scale of global model grid-boxes). A list of products used in this paper is given in Table S1.

The main data is AOD at 550 nm, the wavelength at which models typically provide AOD. If AOD was not retrieved at this wavelength, it was interpolated (or extrapolated) from nearby wavelengths.

[3] AERosol Comparisons between Observations and Models `https://aerocom.met.no`

https://doi.org/10.5194/egusphere-2026-2656
Preprint. Discussion started: 29 May 2026

All products were provided globally for three years (2006, 2008 and 2010, years used in AEROCOM control studies). Many products only provided data over land. Seven datasets belong to sensors that have an equatorial crossing time in the morning, and another nine belong to sensors that have an equatorial crossing time in the afternoon.

The satellite data used in the current study is identical to that used in Schutgens et al. (2020) and, for POLDER[4], Schutgens et al. (2021). It should be noted that the AATSR[5] products have seen new versions appear since then. We decided to continue using the older products to allow continuity. The products most analysed in the current paper (MODIS[6] DarkTarget, MODIS-BAR[7] and POLDER-GRASP[8]) have not seen any upgrades. For POLDER-RemoTAP, we obtained a newer version, as we originally only had data for 2006 (in Schutgens et al. (2021) this product was called POLDER-SRON). The new version of RemoTAP provides data for 2008 and 2010 as well and performs better against AERONET.

2.3 AEROCOM models

The model data used in this paper belong to the AEROCOM Phase III CONTROL experiment, see Table S2. These particular model data were created as part of the Remote Sensing experiment (https://aerocom.met.no/experiments/RemSens) that produced, amongst others, AOD at 550 nm at high temporal frequency (3-hourly) for 2006, 2008 and 2010. CONTROL simulations use nudged meteorology to enable close comparison to observations. These data have been used before, in Zhong et al. (2022, 2023).

2.4 Perturbed Parameter Ensembles and emulators

Two Perturbed Parameter Ensembles are used in this study, based on the global aerosol models UKESM1-A[9] and ECHAM-HAM[10]. The UKESM1-A model (Sellar et al., 2019) is related to the HadGEM model participating in AEROCOM (see Table S2) but includes additional Earth system processes (it uses identical grid resolution). The UKESM1-A PPE (Regayre et al., 2023) has 221 members and 37 perturbed parameters and was run for December 2016 to November 2017. The ECHAM-HAM model (Tegen et al., 2019; Neubauer et al., 2019) is an updated version of the ECHAM-HAM model participating in AEROCOM (see Table S2) (it uses identical grid resolution). The ECHAM-HAM PPE (Bhatti et al., 2026) has 221 members and 23 perturbed parameters and was run for 2010. The PPE members' meteorology was nudged to ERA-Interim reanalysis. A list of perturbed parameters is shown in Table S3 from which we can see there are both similarities and differences in the choice of perturbed parameters. In particular, the ECHAM-HAM PPE is more focused on emission uncertainties while the UKESM1-A PPE is more focused on uncertainties in (aerosol-) cloud processes. Table S3 does not list all UKESM1-A perturbed parameters but only those that are important in the current analysis.

[4]POLarization and Directionality of the Earth's Reflectances
[5]Advanced Along-Track Scanning Radiometer
[6]Moderate Resolution Imaging Spectroradiometer
[7]Bayesian Aerosol Retrieval
[8]Generalized Retrieval of Aerosol and Surface Properties
[9]United Kingdom Earth System Model
[10]European Centre HAmburg Model-Hamburg Aerosol Module

https://doi.org/10.5194/egusphere-2026-2656
Preprint. Discussion started: 29 May 2026

The value range of parameter perturbations is based on expert elicitation (Lee et al., 2013) and prior work on PPEs (Regayre et al., 2018; Yoshioka et al., 2019; Johnson et al., 2020). Values are selected using Maximin Latin hypercube sampling (Lee et al., 2013) which distributes those values as evenly as possible across parameter space. Gaussian Process emulators (O'Hagan, 2006) were constructed for regional, yearly AOD and autocorrelations, using the ESEm[11] package (Watson-Parris et al., 2021a). Emulator skill was assessed in the usual way, by estimating AOD and autocorrelations for one PPE member after being trained on the other 220 members, and repeating this for all members. The ECHAM-HAM emulator showed significantly higher skill than the UKESM1-A PPE, likely due to the larger number of perturbed parameters for the same ensemble size.

A-priori parameter value distributions and the emulators were used to construct ensembles of 1 million variants for either the UKESM1-A or ECHAM-HAM model that will be analysed in Sect. 4. It is not our purpose to compare these two emulators but rather to show that irrespective of model and perturbed parameter choices, similar conclusions may be drawn with respect to the information content of autocorrelations.

2.5 Collocation procedure

To reduce representation errors (Colarco et al., 2014; Schutgens et al., 2016a, b, 2017) in our analyses, all data will be collocated in space and time. Observational datasets are aggregated to the same spatio-temporal grid $1^o \times 1^o \times 3^{\mathrm{hr}}$, after which collocation is achieved by retaining only data available at the same times and locations in all relevant datasets (a simple masking operation). Model data is linearly interpolated to times and locations of available super-observations. More details can be found in Appendix A of Schutgens et al. (2020). Representation errors are not eliminated by this procedure, as the field-of-view of AERONET sites is very limited (Schutgens, 2020), the satellite $1^o \times 1^o$ is seldom fully covered and the model grid-boxes vary from $0.5^o \times 0.5^o$ to $2^o \times 3^o$. In addition there will be small time differences between satellite products and AERONET data (maximally 3 hours but usually less). Our previous work (and the analyses in this paper) suggest that our collocation procedure strongly reduces representation errors. At some locations, representation errors will exhibit biases due to prevailing aerosol spatial distributions and seasonalities (Schutgens, 2020). This is unavoidable due to the differences in spatial representativeness of our datasets. Our use of *regional* averages in this paper should mitigate this issue.

Although satellite sampling is expected to affect the absolute value of autocorrelations, we will evaluate the robustness of the information that can be drawn from climatological patterns and the implications for climate models. See Sect. S2 for more detail.

2.6 Autocorrelations

For a finite, discrete time-series f_i of N elements at times t_i with constant timestep $\Delta t = t_{i+1} - t_i$, we can rewrite Eq 2 as:

$$\rho(k\Delta t) = \frac{< (f_i - \mu)\,(f_{i+k} - \tilde{\mu}) >}{\sigma\tilde{\sigma}} = \frac{< f_i f_{i+k} > - \mu\tilde{\mu}}{\sigma\tilde{\sigma}} \tag{4}$$

[11] Earth System Emulator, `https://github.com/duncanwp/ESEm`

https://doi.org/10.5194/egusphere-2026-2656
Preprint. Discussion started: 29 May 2026

where $<>$ now indicates a time average over only part of the time-series $i = 1 \ldots N-n$, and $n\Delta t$ is the maximum lag and $k\Delta t$ is the specific lag at which we calculate the autocorrelation ($0 \leq k \leq n$). The mean μ and standard deviation σ are calculated for f_i while $\tilde{\mu}, \tilde{\sigma}$ are calculated for f_{i+k}.

In case of a discrete time-series f_i of N elements at times t_i with a varying time separation $t_{i+1} - t_i > 0$ we can define a nominal time-step Δt. This nominal time-step might be the average time-step or the minimum typical time-step, for example 1 day for Low-Earth-Orbit platforms. We can now create two subsets of f_i called g_j and $\tilde{g}_j$ with $j = 1 \ldots N-n$ and $|\tilde{t}_j - t_j - k\Delta t| \leq \frac{1}{2}\Delta t$. These subsets are two series shifted in time by (nominally) $k\Delta t$. The value of n is no longer related to a maximum lag but rather is set by the specific time ordering of the original series and the condition $|\tilde{t}_j - t_j - k\Delta t| \leq \frac{1}{2}\Delta t$. It is likely that n will vary with k (which determines the lag). In any case, we can now write the autocorrelation as:

$$\rho(k\Delta t) = \frac{< g_j \tilde{g}_j > - \mu\tilde{\mu}}{\sigma\tilde{\sigma}} \tag{5}$$

where μ, σ are the mean and standard deviation calculated for g_j and $\tilde{\mu}, \tilde{\sigma}$ are calculated for $\tilde{g}_j$.

The irregular time sampling is a form of sub-sampling and will have an impact of the value on ρ. Fortunately, it is possible to estimate the impact of this sub-sampling through model studies as in Sect. S2. More-over, as long as the sub-sampling is applied consistently (i.e. applied equally in all datasets that are used in an analysis), no negative impacts are expected.

As suggested, Eq. 5 can also be used for satellite observations. However, revisit times of the same location may be several days (depending on orbits, swath width, cloudiness and various factors affecting success of the retrieval), leading to low data counts. We solve this by swapping space for time: all time-series within a region (see Fig. 1) will be used to calculate the autocorrelation. This is achieved by including all data over a region in f_i while ensuring that individual $g_j \tilde{g}_j$ always refer to the same location ($1^o \times 1^o$ grid-box). The impact of the sub-sampling and the space-time trade is investigated in Sect. S2.

2.7 Regions of interest

Figure 1 shows the regions for which we will conduct our analyses. We have chosen rather large regions, known for particular aerosol typologies. They correspond to the regions used in Schutgens et al. (2020) and Schutgens et al. (2021). The analyses presented in this paper can be made for smaller regions but at the moment we only want to present a broad overview.

3 Timescales in a simple box model

In this section, we develop a conceptual model for autocorrelations using a simple box model. This simple box model (Jacob, 1999) can be used to generate time-series:

$$\frac{dm(t)}{dt} = S(t) - km(t), \tag{6}$$

where $m(t)$ is the mass inside a box, $S(t)$ the source of this mass (which could be any combination of emission, production and inflow) and k is the rate constant for first order loss processes due to deposition, destruction and outflow. In equilibrium, $m = S/k$ and the lifetime associated with this system is $T = 1/k$.

https://doi.org/10.5194/egusphere-2026-2656
Preprint. Discussion started: 29 May 2026

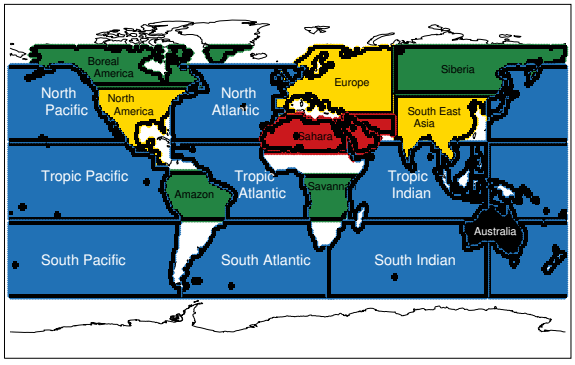

Figure 1. Regions considered in this study. Colours indicate aerosol typologies: marine (blue), dust (red), industrial (yellow), biomass burning (green). The Pacific regions extend west (left) of the dateline. The Middle East region is not labelled but can be seen between Sahara and South East Asia regions. The Australia region is in black since it was flagged as a particularly challenging region for retrievals in Schutgens (2020), see also Sayer et al. (2014).

In this paper, we take this box to be the entire atmospheric column over large areas, like in Fig. 1. The loss rate constant $k = k_d + k_o$ is the sum of two separate loss rates k_d due to deposition (and destruction) and k_o due to outflow. We assume that a fairly typical loss rate for deposition (and destruction) is given by the *global* lifetimes as estimated by AEROCOM models that vary from 3 to 9 days, and are usually less than 1 day over remote oceans (Textor et al. 2006, Gliss et al. 2021), although there may be strong regional variations (Schutgens and Stier, 2014). The lifetimes associated with outflows are undocumented in AEROCOM models, but can be estimated from typical windflow speeds v and box sizes L as L/v. From ERA5 data, we estimate that typical windspeeds at 100 m above the surface over land and ocean are ~ 2.5 m/s vs ~ 7.5 m/s.These windspeeds are dominated by the longitudinal component. For a box with a size of $L = 3000$ km, we then arrive at outflow related lifetimes of 13.8 days over land and 4.6 days over ocean. Over high southern latitudes, oceanic windspeeds may be substantially larger (~ 15 m/s) but so are our boxes (see Fig. 1). Consequently, lifetimes $1/k$ over large areas will be dominated by deposition although some contribution from outflow may be expected.

Consider now a system that has been in equilibrium for an infinite amount of time, but at $t = 0$ we add an instantaneous pulse to the source, $S(t) = S_0 + \Delta m\,\delta(t)$, where $\delta(t)$ is the Dirac delta. The solution is

$$m(t) = \begin{cases} m_0 = \dfrac{S_0}{k} & \text{if } t < 0 \\ m_0 + \Delta m\, e^{-kt} & \text{if } t \geq 0 \end{cases} \tag{7}$$

Applying Eq. 2 for autocorrelations, we find $\rho(\tau) = e^{-k\tau}$. This implies that the decorrelation time is equal to the lifetime of the system: $\tau^* = T$.

If we now consider a system in equilibrium that is perturbed by a rectangular pulse of duration Θ, the mathematics become substantially more complicated but it can be shown that the decorrelation time is a non-linear function of Θ and the lifetime

https://doi.org/10.5194/egusphere-2026-2656
Preprint. Discussion started: 29 May 2026

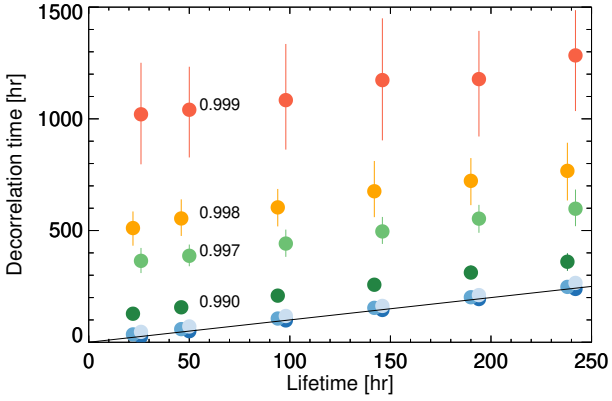

Figure 2. Decorrelation times τ_m^* versus lifetimes $T = \frac{1}{k}$ for several parameter combinations (c_S, k) in the simplebox model Eq. 6. Shown are averages over a sample of 100 times-series, with the bars indicating one standard deviation. Colors indicate c_S values (some values are also shown; dark to light blue refers to $c_S = 0.5, 0.9$ and 0.95). The black line represents $y = x$.

(and nothing else, see Section S1). In nature, we expect Θ to often be much greater than the lifetime: examples are dust or fire seasons that last a month or longer and project a strong seasonality in the source term $S(t)$. Based on algebraic and numerical analysis, we expect the magnitude of the decorrelation time to be dominated by Θ. The lifetime can, in principle, still be estimated from autocorrelations, since $\rho(\tau \geq \Theta) = e^{-k\tau}$.

We also consider numerical simulations of $m(t)$ for the case of a time-varying source $S(t) > 0$. The source is generated from a simple autoregressive AR(1) model or first order auto-regressive process, see Box et al. (2016),

$$S_t = c_S S_{t-1} + \epsilon_t \tag{8}$$

with ϵ_t uncorrelated random noise and $0 < c_S \leq 1$. This results in a time-series of random but correlated $S(t) > 0$, with a correlation c_S after one time-step (we will use a time-step of 1 hour). The integration of Eq. 6 is done with a 4^{th}-order Runge-Kutta method (Press et al., 1989). The initial conditions are the equilibrium values $S(t = 0) = S_0$ (which will also be the mean $< S(t) >$) and $m(t = 0) = m_0 = S_0/k$. The parameters of this system are $0 < c_S \leq 1$ and $k > 0$, which we may freely choose. Without limitation to our analysis, we choose $S_0 = 1$ and rescale $S(t)$ so that it has a standard deviation of 0.2 (independent of c_S). Example time-series of $S(t)$ and $m(t)$ are shown in Fig. S1.

For several parameter combinations (c_S, k) we generate 100 time-series of $S(t)$ and $m(t)$ and calculate both the lifetime and decorrelation time for $m(t)$. Results are shown in Fig. 2. We see that for low correlations in $S(t)$, the decorrelation time for $m(t)$ (τ_m^*) is very similar to the lifetime T. However, for high correlations in $S(t)$, the decorrelation time tends to be higher than the lifetime for T. In that case, the slowly varying source term $S(t)$ strongly affects the time evolution of $m(t)$.

A decorrelation time τ_S^* for the $S(t)$ fluctuations can be estimated from Eq. 4 and varies from about 1.5 hours to 1000 hours for our choices of c_S (with higher c_S implying higher τ_S^*). Interestingly, $\tau_m^* - \tau_S^*$, which is the decorrelation time of $m(t)$ minus the decorrelation time of $S(t)$, agrees very well with the lifetimes, see Fig. 3.

https://doi.org/10.5194/egusphere-2026-2656
Preprint. Discussion started: 29 May 2026

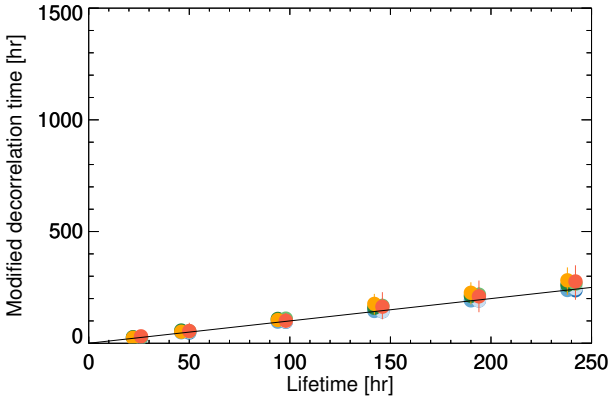

Figure 3. Modified decorrelation time $\tau_m^* - \tau_S^*$ versus lifetime $\frac{1}{k}$ for the same parameter combinations (c_S, k) as in Fig. 2. The black line represents $y = x$.

Further numerical experiments are shown in Fig. S2 where the source S is generated from an auto-regressive process as before but also has a finite-width rectangular pulse imposed on it. The decorrelation time is then defined by three time-scales $(T, \tau_S^*$ and $\Theta)$ as well as the relative amplitude of the random noise and the pulse.

Our conclusion is that decorrelation times are a complex mixture of the time-scales relevant to the aerosol: the lifetime set by deposition (with a minor contribution from outflow) and the multiple time-scales present in emission and/or inflow (daily/weekly fluctuations and seasonal events). For certain circumstances, it appears possible to estimate lifetimes from decorrelation times, provided enough is known about the variation of emissions (and inflow).

4 Which aerosol processes affect temporal autocorrelations?

In this section we investigate which aerosol processes determine autocorrelations. Conversely, observations of these autocorrelations can help us improve those processes in global models. Although it may be difficult to estimate lifetimes from autocorrelations (Sect 3), autocorrelations will be shown to nevertheless provide useful and novel information. Our primary dataset for the analyses in this section consists of two Perturbed Parameter Ensembles, see Sect. 2.4 .

Figure 4 shows a fractional variance analysis for yearly AOD and the temporal autocorrelation at a lag of 6 days (ρ_6) for the ECHAM-HAM PPE, for the regions defined in Sect. 2.7. Such an analysis shows how much the uncertainty in different processes (here represented by perturbed model parameters) contributes to the overall uncertainty in AOD or ρ_6. The first thing to notice is that the same processes are important for AOD and ρ_6 variance, although their relative contributions can be quite different.

For example for the Sahara region, dust emission (EMI_DUST, see Table S3 for definitions) almost completely determines the variance in AOD but it matters much less to ρ_6 whose variance comes from several parameters, including biomass emissions (EMI_BB) and dust absorption (DU_RAD_NI). For the Australia region, seasalt emissions (EMI_SSA) are the most important

https://doi.org/10.5194/egusphere-2026-2656
Preprint. Discussion started: 29 May 2026

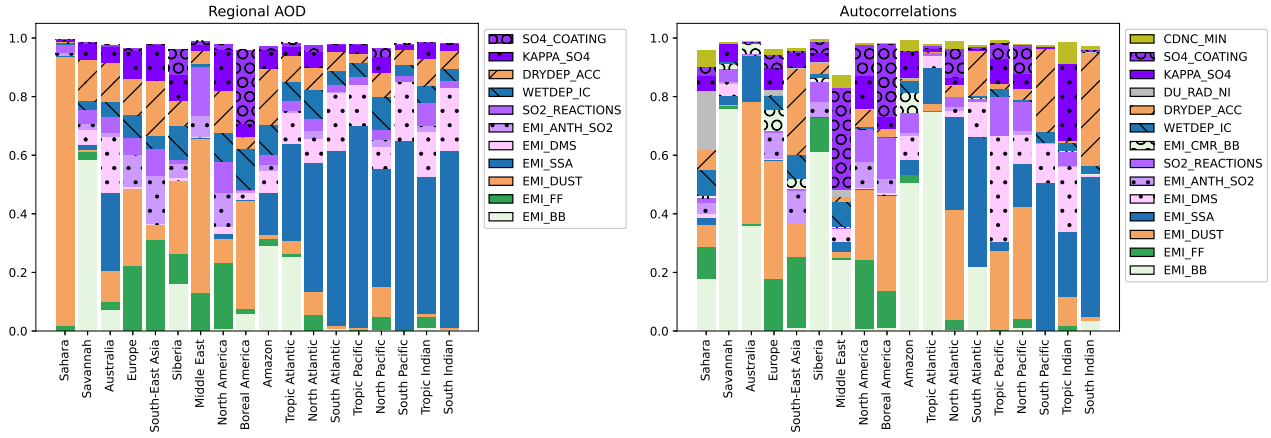

Figure 4. Fractional variance in modelled AOD (left) and ρ_6 (right) as derived from the ECHAM-HAM emulators for various regions. Only fractional variances > 0.05 are shown.

process for AOD variance but dust emissions (EMI_DUST) dominate ρ_6. As a matter of fact, biomass emissions (EMI_BB) are more important to ρ_6 than seasalt emissions (EMI_SSA). For the Siberia region, dust emissions (EMI_DUST) are the dominant process for AOD variance, but they barely affect ρ_6 where biomass emissions (EMI_BB) causes about 60% of the variance. Likewise in the Tropical Atlantic ocean region, seasalt emissions (EMI_SSA) are the dominant process for AOD variance, but it matters much less for ρ_6 where biomass emissions (EMI_BB) accounts for about 70% of the variance. In the southern oceanic regions, dry deposition of accumulation mode (DRYDEP_ACC) is significantly more important to ρ_6 than to AOD variance. We can interpret these findings in the context of the simple box model. For very clean regions (Hamilton et al., 2014) with relatively little inflow like the southern oceanic regions, it is unsurprising that deposition processes (strongly related to k_d in Sect. 3) have a large impact on ρ_6. However, seasonal inflow of biomass burning aerosol can explain the results for the Tropical Atlantic ocean, where the ρ_6 variance is strongly impacted by biomass burning emissions, similar to how seasonal events affected ρ in Sect. 3.

We can also look at how the two dominant processes affect AOD and ρ_6 per region. For a few representative regions, we provide examples in Fig. 5. For the Europe and North America regions, the fractional variance analysis in Fig. 4 does not suggest substantial differences between AOD and ρ_6. But Fig. 5 shows that AOD and ρ_6 for these two regions react differently to changes in either fossil fuel (EMI_FF) or dust (EMI_DUST) emissions. In particular, if we knew the value of AOD (represented by an arbitrary contour line for AOD), this would not constrain these processes (their parameters) very much. But if we knew both AOD and ρ_6, fossil fuel and dust emissions could be constrained significantly for the ECHAM-HAM model. We see something similar for the South Indian ocean region, but now for seasalt emissions (EMI_SSA) and dry deposition of the accumulation mode (DRYDEP_ACC). Only for the Boreal America region do AOD and ρ_6 seem not to provide complementary information (at the moment, we do not have an explanation for this; ρ_6 may contain information on another, less important, model processes but that was not explored). A similar situation exists for the Savannah (not shown).

https://doi.org/10.5194/egusphere-2026-2656
Preprint. Discussion started: 29 May 2026

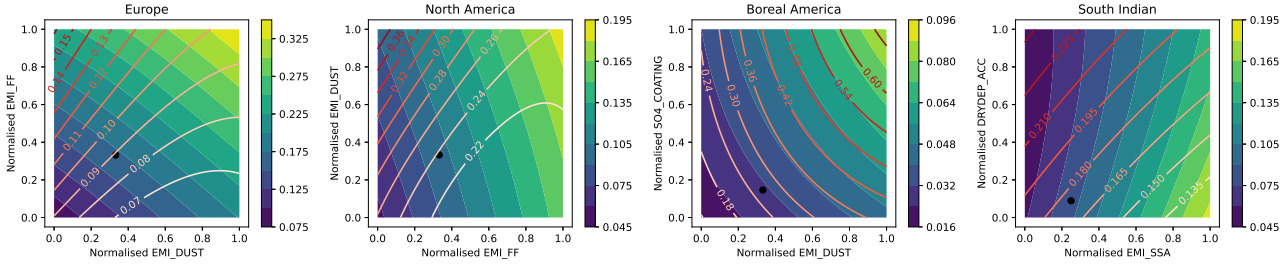

Figure 5. Dependence of AOD and ρ_6 in ECHAM-HAM on dominant parameters for selected regions. AOD is shown as a filled contour map that uses the colourbar on the right. ρ_6 is shown as contour lines with labelled values. Here the parameter values have been normalised according to their max-min spread across the ensemble of 1 million variants of ECHAM-HAM. The black dot represents the default parameter choice.

We conclude that ρ_6 contains information independent from AOD, and that it seems possible to interpret ρ_6 using the conceptual model developed in Sect. 3.

A similar analysis can be made for UKESM1-A. Our purpose is not to compare UKESM1-A to ECHAM-HAM (their PPEs were built for different purposes and used different combinations of perturbed parameters) but to see if, again, ρ_6 contains useful information that may be interpreted through our conceptual model. Figure 6 shows the fractional variance analysis for UKESM1-A, that again suggests similar processes matter for AOD and ρ_6 variance, but their impact on variances is different. For the Australia region, seasalt emissions (sea_salt) matter for AOD but not for ρ_6 which is instead controlled by SOA production from monoterpene (bvoc_soa) and dry deposition of the accumulation mode (dry_dep_acc). Over the Europe region volcanic SO_2 emissions (volc_so2) matter greatly for ρ_6 but not to AOD, just like the emitted size of primary SO_4 (prim_so4_diam) matters greatly to ρ_6 for the South East Asia region but not to AOD. For the North and Boreal America regions, ρ_6 is strongly affected by SOA production from monoterpenes (bvoc_soa) but AOD not so much. Again we see the stronger impact from a deposition process (dry_dep_acc) on ρ_6 than on AOD over remote ocean regions. In UKESM1-A dust emissions were not perturbed, so the impact due to seasonal inflow on ρ_6 as seen in the ECHAM-HAM PPE (for the North Atlantic, Tropical and North Pacific ocean regions) is absent. In contrast, there is a markedly strong impact from dimethyl sulfide (dms) emissions on the oceanic ρ_6 (but not AOD). This is possible if dms emissions have a strong seasonal cycle that influences autocorrelations (Bhatti et al., 2023, 2024).

Also for the UKESM1-A PPE, we conclude that ρ_6 contains information independent from AOD, which is further explored in Fig.7. Again we see that the two processes that dominate variance in AOD and ρ_6 often have a very different impact allowing us to constrain their parameters from observations of AOD and ρ_6 together, but not separately.

To conclude, these analyses provide a wealth of evidence that ρ_6 contains independent and additional information to regional AOD, on important aerosol processes. In particular, processes that sensitively affect ρ_6 like fossil fuel, biomass burning, seasalt and DMS emissions as well as accumulation mode dry deposition (EMI_FF, EMI_BB and EMI_SSA in ECHAM-HAM and sea_salt, dry_dep_acc, and dms in UKESM1-A) are known to contribute significantly to the uncertainty in global aerosol

https://doi.org/10.5194/egusphere-2026-2656
Preprint. Discussion started: 29 May 2026

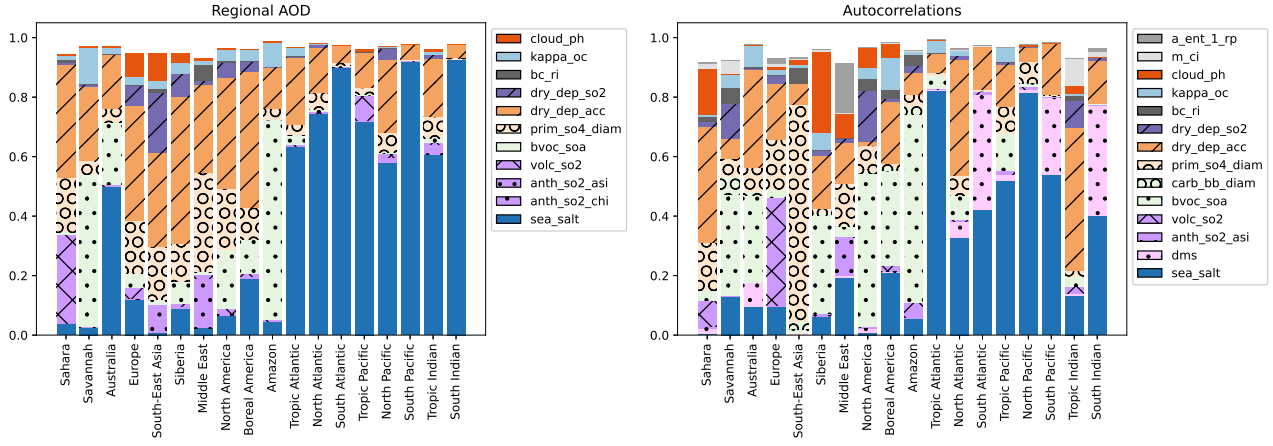

Figure 6. Fractional variance in modelled AOD (left) and ρ_6 (right) as derived from the UKESM1-A emulators for various regions. Only fractional variances > 0.05 are shown.

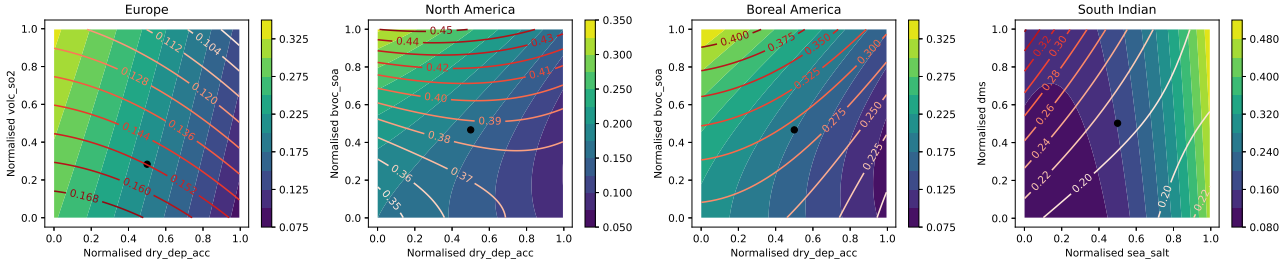

Figure 7. Dependence of AOD and ρ_6 in UKESM1-A on dominant parameters for selected regions. AOD is shown as a filled contour map that uses the colourbar on the right. ρ_6 is shown as contour lines with labelled values. Here the parameter values have been normalised according to their max-min spread across the ensemble of 1 million variants of UKESM1-A. The black dot represents the default parameter choice.

forcing (Regayre et al., 2026; Bhatti et al., 2026). The fact that the two PPEs give different results as to which parameters can be estimated is not relevant to this conclusion. That is the result of the PPEs being different, both with respect to the actual model, and to the parameters that are perturbed.

5 Evaluation of satellite observed autocorrelations

Satellite observed autocorrelations can be evaluated with AERONET measurements. In this section, super-observations of AOD are first collocated with AERONET observations (see Sect. 2.5), after which autocorrelations will be calculated for the collocated data in individual regions according to Sect. 2.6.

https://doi.org/10.5194/egusphere-2026-2656
Preprint. Discussion started: 29 May 2026

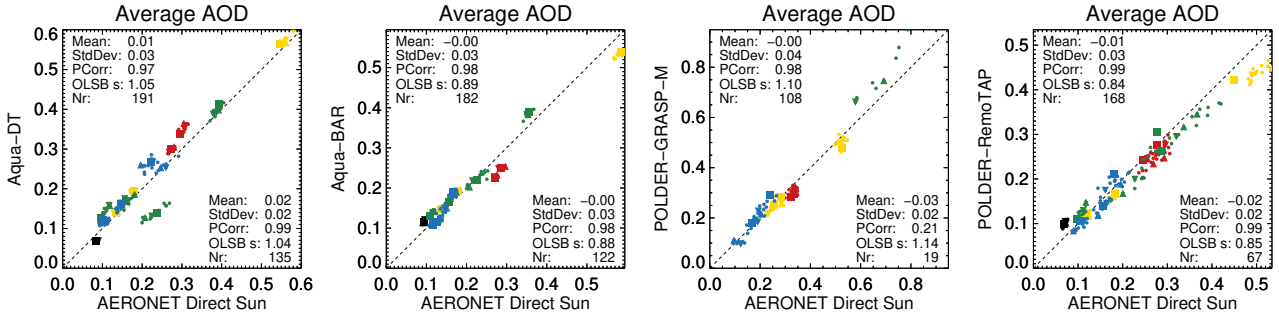

Figure 8. Evaluation of satellite observed regional averaged AOD with AERONET. Each symbol is the regional AOD for a specific region and lag. Colours indicate regions (red: deserts, blue: ocean, green: biomass burning, yellow: North America, Europe, South-East Asia, black: Australia). Symbols indicate lags (upward triangle: 3 days, square: 6 days, downward triangle: 9 days, dots: all other lags from 1 to 14 days). Statistics are shown for symbols based on at least 30 data pairs (upper left) or at least 300 (lower right). The mean, standard deviation, Pearson correlation, an unbiased slope estimate (OLSB) and the number Nr of regions/lags are shown. The dashed black line represents $y = x$.

The evaluation of regional averaged AOD for four satellite products can be seen in Fig. 8, showing an excellent agreement with AERONET. Such agreement is seldom seen in standard evaluations of satellite observations, and is here achieved through the substantial spatio-temporal averaging of (collocated) data that removes random error contributions (both retrieval and representation errors). Even so, some sizeable biases can be seen, for example for Aqua-DT (DarkTarget) over the Savannah (cluster of green points below $y = x$). Results for all satellite products are shown in Fig. S6.

Figure 9 shows the evaluation of autocorrelation for the same four products. Although the same data were used in both analyses, the evaluation appears noisier than for regional AOD in Fig. 8. Regional averaged AOD will mostly suffer from biases in the AOD super-observations while autocorrelations will suffer mostly from random errors. This is a direct consequence of the mathematical properties of averages and autocorrelations. Consequently, Figs. 8 and 9 provide complementary information on the performance of satellite products.

As for the satellite observed autocorrelations, overall there is good agreement with AERONET. In particular, AERONET confirms the wide range of autocorrelations for biomass burning regions, the clustering of autocorrelations around 0.2–0.4 for desert regions and 0.3 for North America, Europe and South-East Asia. Similarly, AERONET confirms the low autocorrelations (≈ 0.1) that can be found for most (but not all) oceanic regions. Results for all satellite products are shown in Fig. S7. They show similar results as Fig. 9, although often a bit noisier. The individual evaluations can't be compared amongst each other because the underlying sampling is different: different orbits, swath widths and masking (due to e.g. clouds) result in large differences in the spatio-temporal sampling of the datasets (collocated with AERONET), see also Fig. S4. Nevertheless, our analysis suggests that in particular the MODIS and POLDER products are capable of observing autocorrelations.

Since averaging seems to be so important, we consider the impact of the number of data pairs used on the errors in satellite observed autocorrelations in Fig. 10. Clearly, these errors decrease as the data count increases, a sign of the presence of

https://doi.org/10.5194/egusphere-2026-2656
Preprint. Discussion started: 29 May 2026

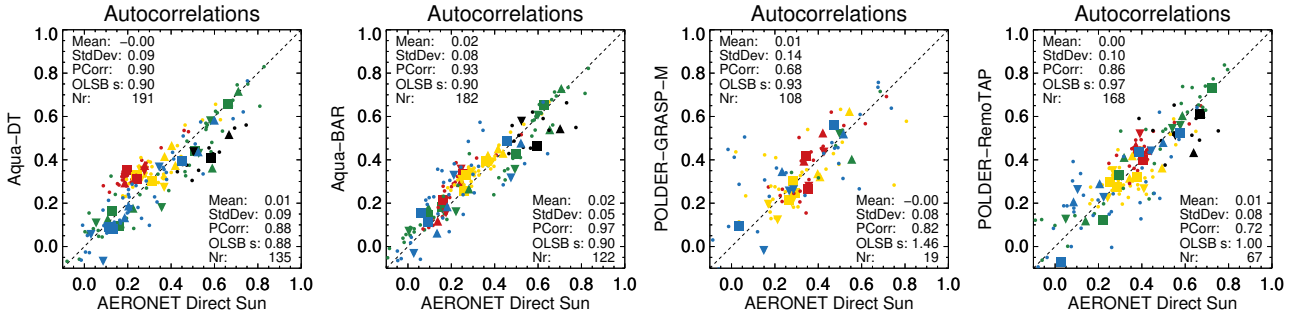

Figure 9. Evaluation of satellite observed autocorrelations with AERONET. Each symbol is the correlation for a specific region and lag. For more explanation, see the caption to Fig. 8

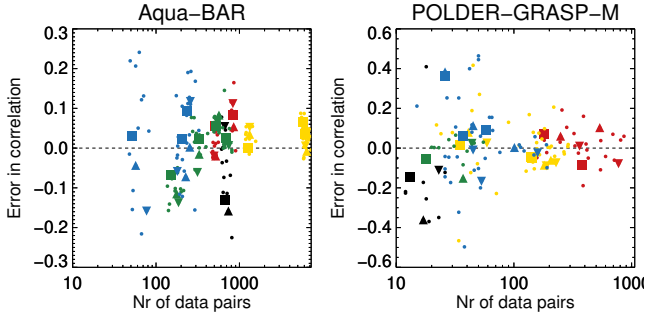

Figure 10. Impact of data count on satellite errors (satellite ρ - AERONET ρ) in Fig. 9. See caption of Fig. 9 for more explanation. Note that AOD retrievals over Australia (black) are known to be problematic (Sayer et al., 2014; Schutgens et al., 2020).

substantial random errors in AOD. This partly explains why GRASP and RemoTAP show larger errors than the Aqua products: they have fewer collocations with AERONET and the data count is substantially lower, in particular for the biomass burning and oceanic regions.

6 Comparison of satellite observed autocorrelations

In this section we compare satellite observed autocorrelations between satellite products, in the hope of improving our understanding of the robustness and accuracy of these measurements. Although the comparison in this section is not fundamentally different from the evaluation in the previous section, a couple of changes are worth noting: 1) there will be many more collocated data, hopefully reducing noise; 2) the data will be more spread out over a region, increasing its representativity (this is especially true over ocean: in Sect. 5, data from AERONET only exist near the coast or on islands); 3) there is no longer a clear 'truth' dataset (in Sect. 5, we implicitly assumed that AERONET observed autocorrelations have negligible errors compared to their satellite counterparts); 4) the impact of representation errors on observed autocorrelations should be reduced as we no longer compare satellite super-observations to point observations from AERONET.

https://doi.org/10.5194/egusphere-2026-2656
Preprint. Discussion started: 29 May 2026

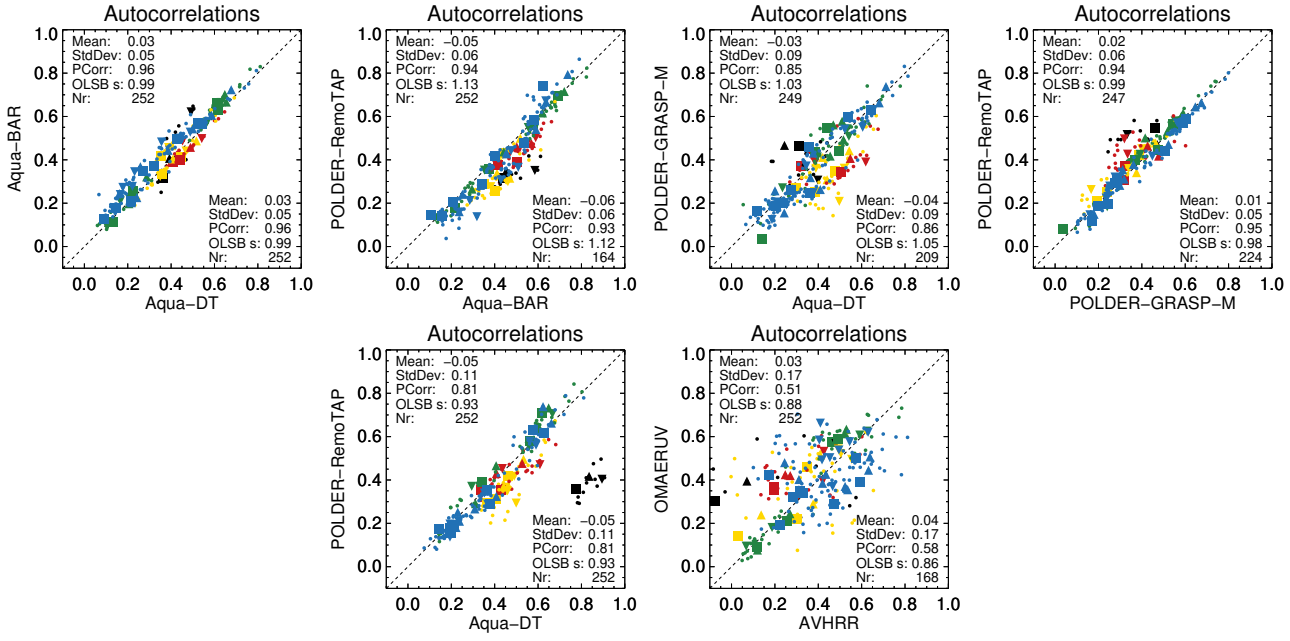

Figure 11. Comparison of satellite observed autocorrelations. Each symbol is the correlation for a specific region and lag. Colours indicate regions (red: deserts, blue: ocean, green: biomass burning, yellow: North America, Europe, South-East Asia, black: Australia). Symbols indicate lags (upward triangle: 3 days, square: 6 days, downward triangle: 9 days, dots: all other lags from 1 to 14 days). Statistics are shown for symbols based on at least 300 data pairs (upper left) or at least 3000 (lower right). The mean, standard deviation, Pearson correlation, an unbiased slope estimate (OLSB) and the number Nr of regions/lags are shown. The dashed black line represents $y = x$. This figure is similar to Fig. 9 but the lower thresholds for minimum data pairs are $10\times$ higher. In this analysis the Australia region is included. Bias and standard deviation for RemoTAP vs Aqua-DT change to -0.02 resp. 0.06 if the Australia region is excluded.

We show a few individual comparisons in Fig. 11. The analyses in this figure mostly show pretty tight agreement between satellite datasets, with the OMEARUV vs AVHRR comparison the obvious exception. A clear example of a bias can be seen for the Australia region between RemoTAP and Aqua-DT. It is unclear which product here is the bigger offender, especially as sampling differs very much from that of the other analyses (e.g. Aqua-DT vs Aqua-BAR or Aqua-DT vs AERONET).

In Sect. 5, we showed that errors in autocorrelations depend on the count of data pairs. These counts substantially increase when comparing two satellite products. For example, in the previous section Aqua-DT evaluation with AERONET was based on typically 733 data pairs per region/lag, with substantial differences between between land and ocean (1,124 vs 119), on account of the dearth of AERONET sites over the latter. In contrast, the comparison of Aqua-DT to RemoTAP, is based on 44,282 (all regions), 36,884 (land) and 53,529 (ocean) data pairs, increases by factors of 60, 33 and 450. This should reduce statistical noise and random contributions to the errors.

Unfortunately, it is also possible that errors in satellite AOD correlate, and lead to a fortuitous cancelling of terms in the Root Mean Square Differences (RMSD) for ρ. However, it is quite hard to see how errors in AOD can correlate for very different

https://doi.org/10.5194/egusphere-2026-2656
Preprint. Discussion started: 29 May 2026

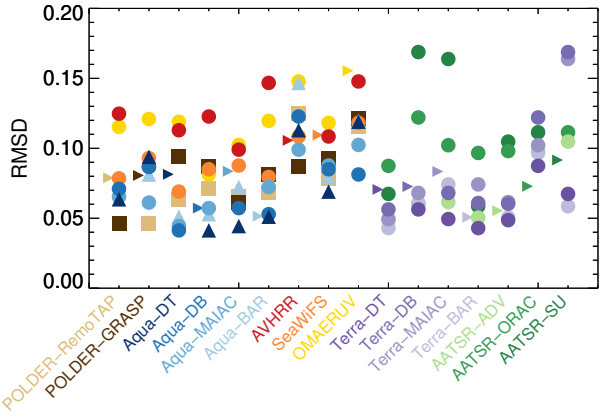

Figure 12. Shown are the RMSD for autocorrelations for all regions/lags, for either two collocated satellite products (vertically stacked symbols) or any satellite product collocated with AERONET (offset right-pointing triangle). Only products with either an afternoon (9 left-most) or morning (7 right-most) over-pass time are compared. The colours of the symbols correspond to different datasets, as shown on the horizontal axis. For increased clarity, MODIS-DT & BAR are further indicated by upward-pointing triangles, and GRASP & RemoTAP by squares. Each RMSD was calculated for a different sampling, as dictated by the collocation of two datasets. Autocorrelations for the Australia region were not included in the RMSD.

sensor/retrieval combinations like RemoTAP & Aqua-BAR or Terra-DT & AATSR-SU. For different retrievals from the same sensor we can study correlations in AOD errors through a triple collocation with AERONET. For Aqua-DT and Aqua-BAR, this triple collocation does not lead to much data loss compared to Sect. 5 and we find that errors in AOD (with respect to AERONET) in DarkTarget and BAR have a low correlation of ~ 0.45. DarkTarget AOD errors (with respect to AERONET) are on average twice as large as those in BAR. In short, we do not believe a fortuitous cancelling of errors is the reason for decreased RMSD for the satellite products shown in Fig. 11.

As a matter of fact, satellite products usually agree better amongst themselves than with AERONET. In Fig. 12 the RMSD are shown for the autocorrelations per region/lag. Each RMSD is calculated from its own collocation of two satellite products or any one satellite product and AERONET. A direct comparison of the RMSD values is consequently hampered by sampling differences, see also Fig. S4. On average, we see a $\sim 30\%$ improvement in RMSD when comparing two satellite products than when evaluating one product with AERONET, but obviously there are substantial differences depending on the products.

We think the analyses presented in this section strongly suggest that satellite observed autocorrelations can have uncertainties of 0.04, at least for the better performing products (e.g. RemoTAP, Aqua-BAR). We arrive at this number by taking a value of 0.06 from Fig. 12 and assuming that both satellite products contribute equally. This uncertainty is supported by the evaluation with AERONET, for example Aqua-BAR has an uncertainty of 0.05. Clearly this is a one-size-fits-all uncertainty estimate and we hope to provide more detailed (product and spatially-aware) uncertainty estimates in the future.

https://doi.org/10.5194/egusphere-2026-2656
Preprint. Discussion started: 29 May 2026

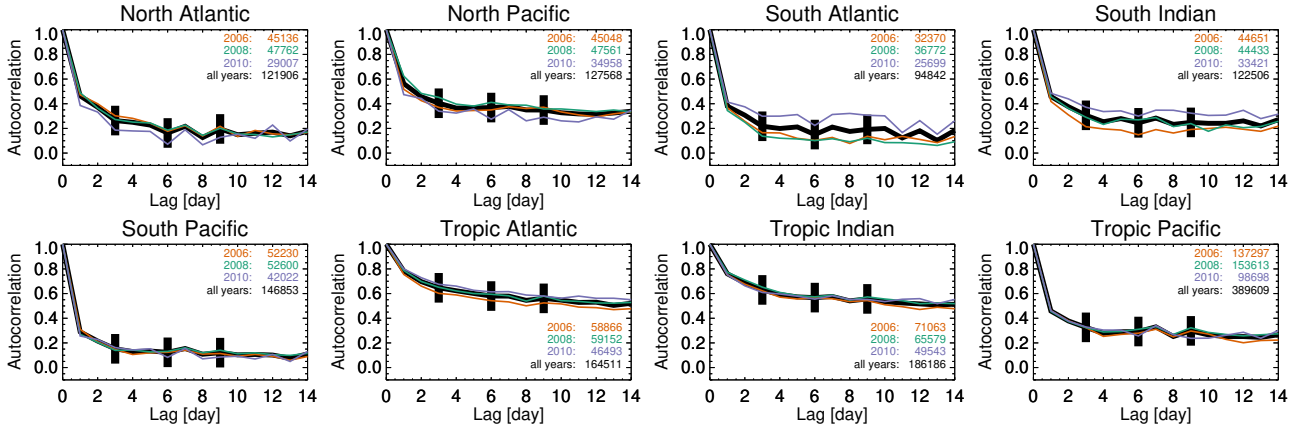

Figure 13. Temporal autocorrelations for a 3-year climatology from RemoTAP (black) and the individual years(colors), for selected ocean regions. Also shown, for lags of 3, 6 and 9 days, are the 3σ uncertainty estimates from Sect. 6. The number of used data pairs is also indicated.

7 A 3-year climatology of global autocorrelations

In this section we will introduce a global 3-year climatology of temporal autocorrelations from RemoTAP, as well results for individual years.

The observations over oceans, see Fig. 13, suggest that southern oceanic regions have very low autocorrelations already from 3 days lag, while northern oceanic regions have slightly higher autocorrelations. The highest autocorrelations, however, are found for the tropical Atlantic and Indian ocean regions and it is tempting to think this may be related to continental outflows that imprint some persistence on the aerosol fields, in contrast to the remote oceans where aerosol emissions fluctuate with windspeeds.

For land regions, see Fig. 14, we see a more varied result. Especially noteworthy is the contrast between the biomass burning regions: the Amazon and the African Savannah regions have high autocorrelations while the Boreal America and Siberia regions have low autocorrelations. This may be related to the length of the biomass burning season which is fairly long in the Tropics and much shorter in the boreal regions.

Similar results for Aqua-DT are shown in Fig. S10 and S11. Aqua-DT has a substantially higher data count than RemoTAP, by factors of 13 (all regions), 6 (land) and 19 (ocean). Results are overall quite similar, with one notable difference: the very low autocorrelations for Aqua-DT over the southern oceans. The differences can to a large extent be explained by the aforementioned sampling differences between the two products, see Fig. S4.

Yearly autocorrelations for RemoTAP are not that different than the 3-year climatology, especially over ocean. For Aqua-DT these differences are even smaller, again suggesting the importance of data count and sampling. See also the analyses in Fig. S5.

Based on the data presented, autocorrelations exhibit strong regional variability, with only limited inter-annual variability.

https://doi.org/10.5194/egusphere-2026-2656
Preprint. Discussion started: 29 May 2026

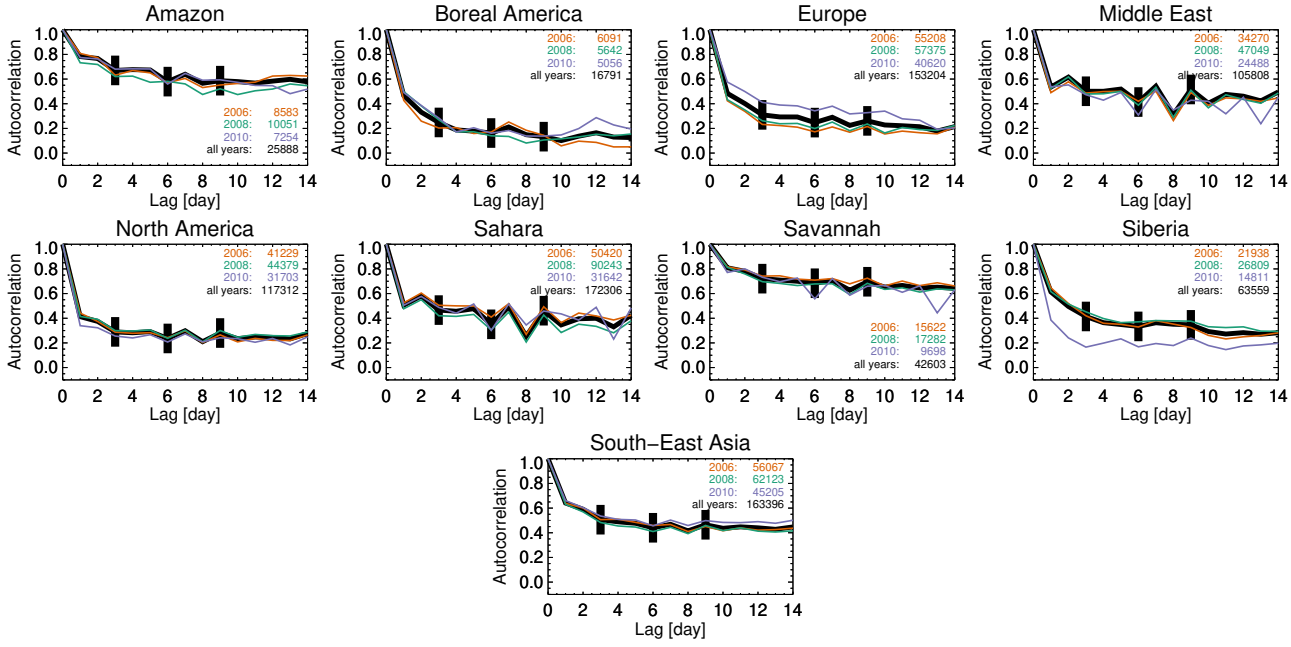

Figure 14. Temporal autocorrelations for a 3-year climatology from RemoTAP (black) and the individual years(colors), for selected land regions. Also shown, for lags of 3, 6 and 9 days, are the 3σ uncertainty estimates from Sect. 6. The number of used data pairs is also indicated.

8 Evaluation of AEROCOM models

Figures 15 and 16 show autocorrelations for various regions from models and the RemoTAP product. Quite generally, autocorrelations decline quickly in the first few days and then reach a plateau. This is true for both the models and observations. The values in the plateau, from a lag of about 6 days and onward, vary significantly from region to region, and from model to model.

In all oceanic regions it is clear that many models overestimate autocorrelations, sometimes quite substantially. Individual models do not show systematic biases across all oceanic regions. For example, HadGEM agrees well with the observations for the Tropical Indian ocean, overestimates it in the Tropical Pacific (although not excessively more than most models), but is a real outlier of overestimation in the North Atlantic.

In Fig. 15 and 16 we also show the $3\sigma = 0.12$ uncertainty range as estimated in Sect. 6. Models that lie outside this 3σ uncertainty range can confidently be considered as predicting incorrect autocorrelations (provided our uncertainty estimate is reasonable). For comparison, actual errors of the observed autocorrelations vs AERONET and differences vs Aqua-BAR) are also shown, to support our 3σ range. Note that we have argued that the errors versus AERONET tend to be on the high side due to low data counts, while the differences versus Aqua-BAR will also be affected by errors in that product. It would appear that temporal autocorrelations have a lot of power to distinguish model performance.

https://doi.org/10.5194/egusphere-2026-2656
Preprint. Discussion started: 29 May 2026

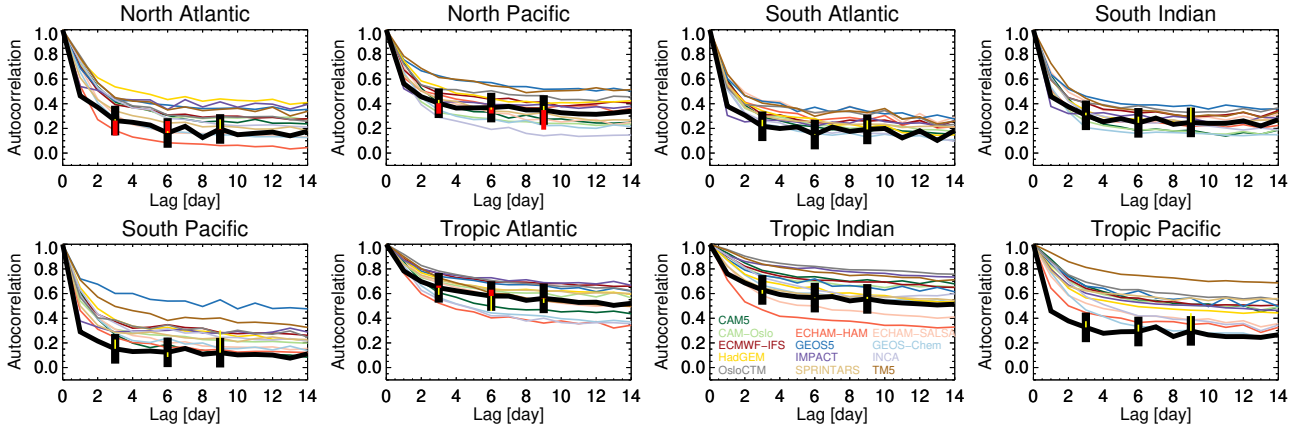

Figure 15. Temporal autocorrelations for AEROCOM models (colours) and RemoTAP (black), for selected ocean regions. Also shown, for lags of 3, 6 and 9 days, are the 3σ uncertainty estimate from Sect. 6, as well as errors vs AERONET (in red, from Sect. 5) and Aqua-BAR (in yellow, from Sect. 6). Note that these uncertainties and errors were estimated for different sampling of RemoTAP.

For comparison, results for Aqua-DT are shown in Figs. S12 and S13. Aqua-DT has a substantially higher data count than RemoTAP, by factors of 13 (all regions), 6 (land) and 19 (ocean). Overall, results are quite similar, and as we argued before, can to a large extent be explained by sampling differences and errors in observed autocorrelations.

The systematic overestimation by models over most regions can be interpreted as follows. According to our conceptual model (Sect. 3), it would appear that modelled timescales in either sources or losses (or both) are too large. Over oceans this might suggest insufficient removal or too large a contribution from outflows (itself caused by insufficient removal or overestimated sources). A more in-depth analysis is out of the scope of this paper and would require constraining processes in models based on observed autocorrelations (a typical PPE exercise).

https://doi.org/10.5194/egusphere-2026-2656
Preprint. Discussion started: 29 May 2026

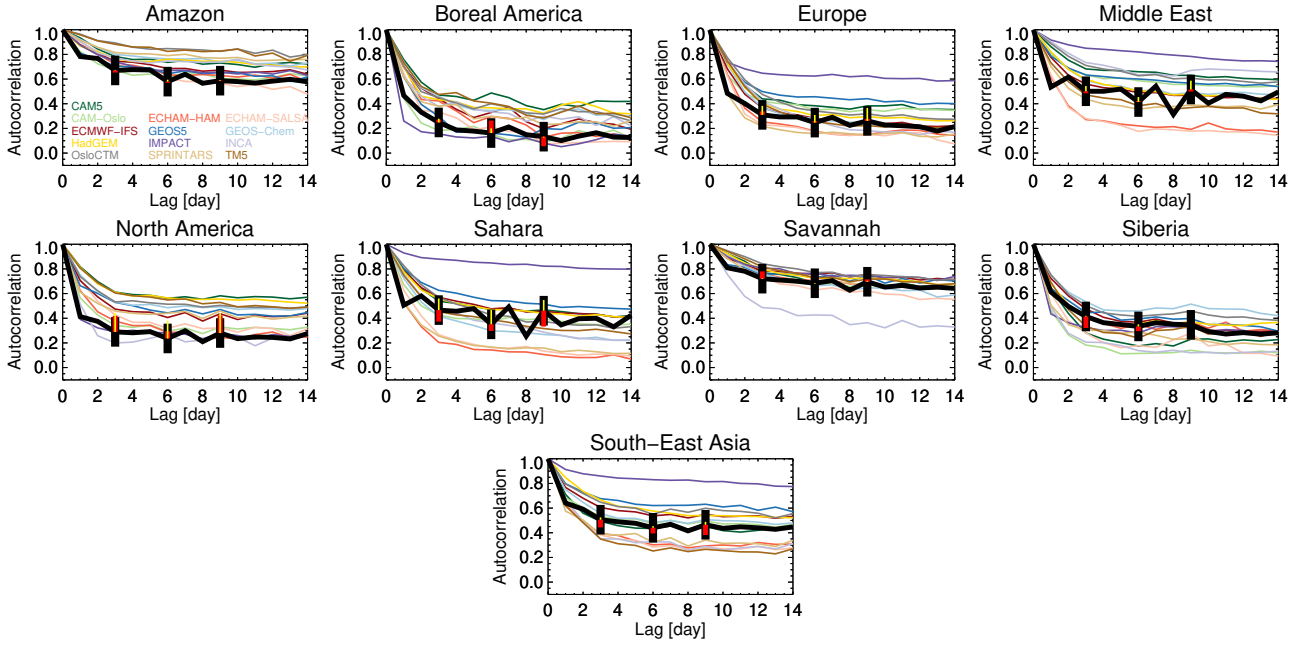

Figure 16. Temporal autocorrelations for AEROCOM models (colours) and RemoTAP (black), for selected land regions. Also shown, for lags of 3, 6 and 9 days, are the 3σ uncertainty estimate from Sect. 6, as well as errors vs AERONET (in red, from Sect. 5) and Aqua-BAR (in yellow, from Sect. 6). Note that these uncertainties and errors were estimate for different sampling of RemoTAP.

The evaluation of individual models at a lag of 6 days (ρ_6) is shown in Fig. 17 and 18. The figures show the evaluation against Aqua-BAR, Terra-DT, AATSR-ADV and RemoTAP. As discussed before, regional autocorrelations will differ amongst products due to varying sampling and different observational errors (the latter was estimated at ~ 0.04, see Sect. 6). To help with the interpretation, regression lines are also shown. Often these match quite closely between the four satellite products. All models show a general agreement with the satellite products but some models show quite a large spread (e.g. ECHAM-HAM, ECHAM-SALSA, IMPACT and INCA) compared to others (e.g. ECMWF-IFS, HadGEM and Oslo-CTM). Several models show a systematic overestimation of the correlation (e.g. ECMWF-IFS, GEOS5-replay, HadGEM. Oslo-CTM) while others show an overestimation at larger modelled autocorrelations but seem fairly unbiased at lower modelled autocorrelations (e.g. CAM5, CAM5.3-Oslo, and IMPACT). This analysis for four datasets is confirmed by most other datasets, see Figs. S8 and S9.

The impact of grid resolution on errors in modelled autocorrelations seems to be unimportant. Of the two models run at high resolution (ECMWF-IFS, $0.7^o \times 0.7^o$, and SPRINTARS, $0.56^o \times 0.56^o$), only ECMWF-IFS shows a small spread (yet still shows a systematic bias). The spread (or bias) of ECMWF-IFS is not very different from that of HadGEM ($1.88^o \times 1.25^o$), a model run at substantially lower resolution. This reaffirms the position that resolution does not solve all climate model issues and there is value in committing resources to other strategies, such as PPEs (Carslaw et al., 2026).

https://doi.org/10.5194/egusphere-2026-2656
Preprint. Discussion started: 29 May 2026

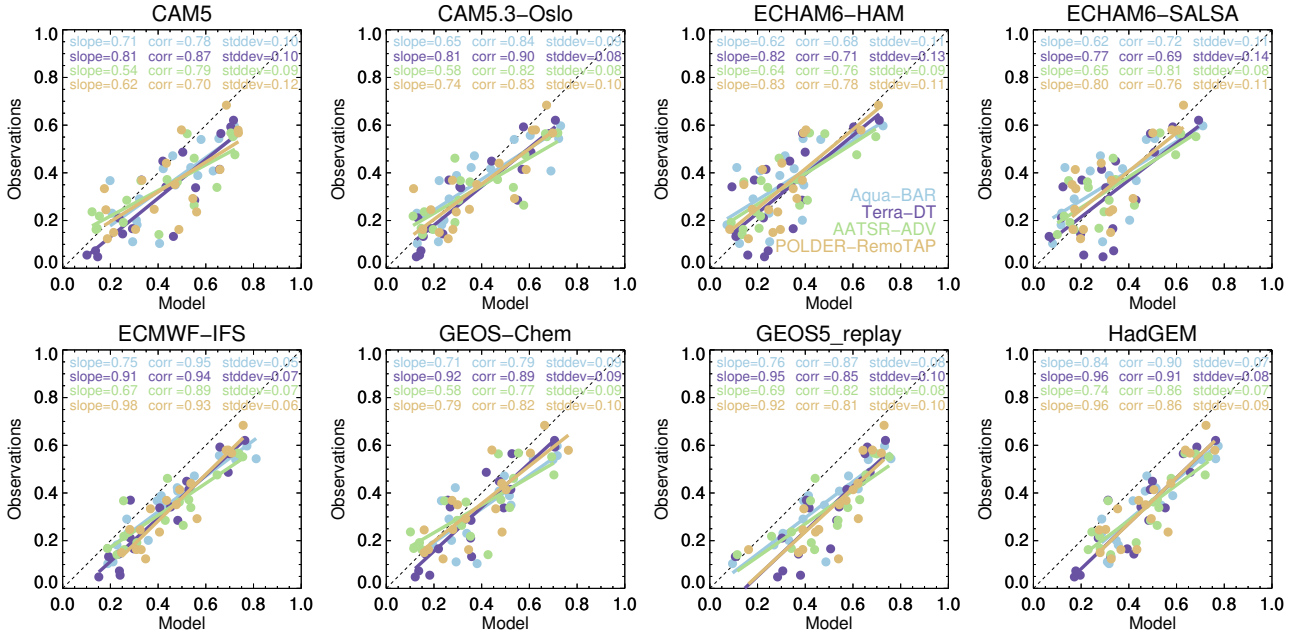

Figure 17. Correlations at a lag of 6 days for individual AEROCOM models and Aqua-BAR, Terra-DT, AATSR-ADV and RemoTAP (for colours, see legend in plot for ECHAM-HAM). Each data point is the lag at 6 days for a specific region. Only region/lag cases with at least 3000 data pairs are shown. The coloured lines are regressions through the available datapoints. The satellite products were used at their original sampling (and the models have been collocated to each product separately).

9 Conclusions

We present a study of temporal autocorrelations (also known as lagged correlations) of aerosol optical depth (AOD). As far as we know, this is the first study to provide a global climatology of temporal autocorrelations. Furthermore, we are the first to develop a conceptual interpretation of autocorrelations and analyse which aerosol processes determine them. Our paper also provides the first ever estimate of the accuracy of satellite observed autocorrelations and an evaluation of AEROCOM modelled temporal autocorrelations. We show that temporal autocorrelations can be calculated from existing datasets yet provide new climatically relevant information.

Using a simple box model for atmospheric aerosol, we infer a relationship between decorrelation times and local aerosol lifetimes. When the sources fluctuate rapidly, the decorrelation time equals the local lifetime. With longer fluctuations in the sources, the decorrelation time depends on both the local lifetime and the timescale for source fluctuations, often in a non-trivial manner. Using two Perturbed Parameter Ensembles (PPEs) for complex state-of-the-art aerosol models (ECHAM-HAM and UKESM1-A) we identify aerosol processes that determine autocorrelations and conversely show how observations of autocorrelations can be used to improve those processes. In particular we show that temporal autocorrelations often contain

https://doi.org/10.5194/egusphere-2026-2656
Preprint. Discussion started: 29 May 2026

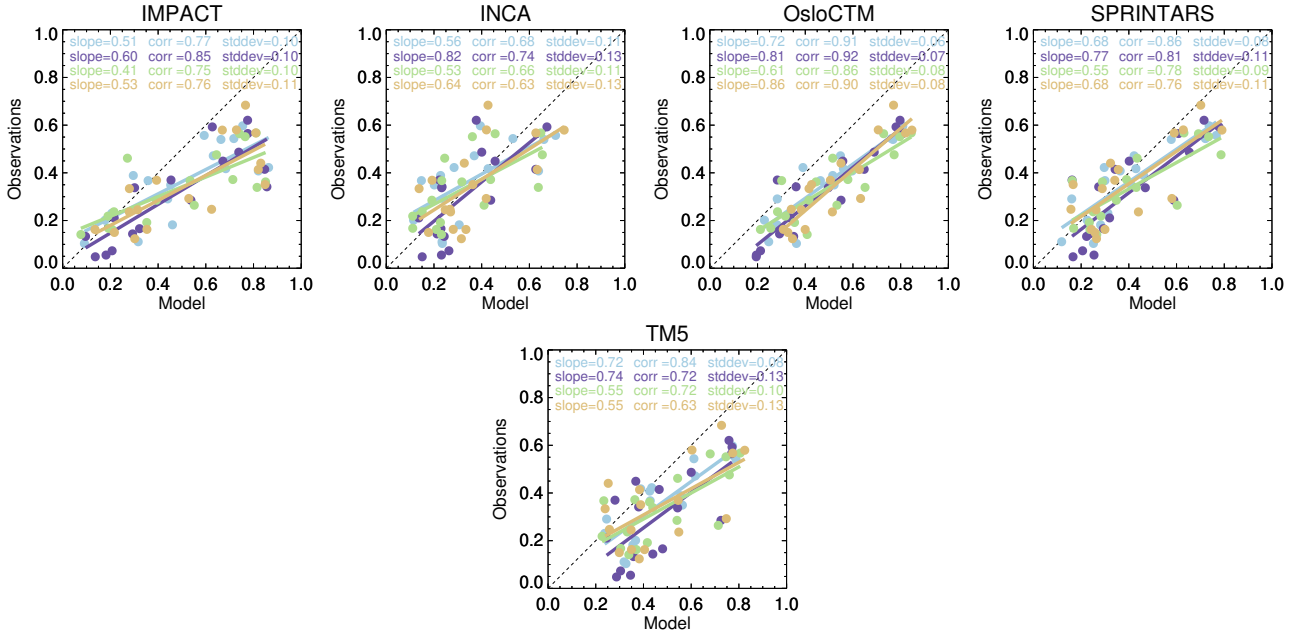

Figure 18. Same figure as Fig. 17 but for different AEROCOM models.

information independent from yearly AOD that should allow a more complete constraining of model parameters, with implications for model skill at simulating future climate.

We show it is possible to construct global observational datasets of temporal autocorrelations from Low-Earth-Orbit spacecraft, even though such platforms have revisit times of one to several days. We provide evidence that the sparse sampling of satellite data does not prevent meaningful interpretation, and evaluate observed autocorrelations from several satellite products against AERONET. We estimate an uncertainty of 0.04 for the better performing satellite products.

Our analysis also suggests that temporal autocorrelations show the strongest change in the first week, and that autocorrelations at 6 days (called ρ_6) may be a useful new metric. The satellite data in general show low ρ_6 over oceanic regions, especially the remote southern regions ($\rho_6 < 0.2$) while well-known outflow regions like the tropic Atlantic and Indian oceans show much higher autocorrelations ($\rho_6 \sim 0.55$). Continental regions generally show higher autocorrelations, with Australia, the Amazon and African Savannah regions showing $\rho_6 \sim 0.6$, industrialised regions (Europe, North-America and Asia) showing $\rho_6 \sim 0.4$ and remote continental regions (Siberia and Boreal America) having $\rho_6 \sim 0.2$.

While interannual variability can be seen in our datasets, we provide evidence that this is more related to limited and varying sampling from satellite than natural variability of the aerosol system. As our dataset only contains data for 2006, 2008 and 2010 we believe changes in ρ_6 over larger periods due to systematically changing emissions are definitely possible.

To conclude our study we evaluate AEROCOM models with satellite observations of autocorrelations. Models tend to significantly overestimate ρ_6 over oceans and many continental regions, although over desert regions, Europe, North America and South-East Asia, different models either under- or overestimate the observations. This suggests that models either underesti-

https://doi.org/10.5194/egusphere-2026-2656
Preprint. Discussion started: 29 May 2026

mate removal of aerosol or overestimate seasonal sources. We do not find evidence of a strong impact from model resolution on its capability to model ρ_6.

Our study suggests various avenues for further research. The simple box model may be used to explore a greater variety of scenarios to better understand how autocorrelations are related to time-scales in local emissions or inflow. The PPEs (and emulators) may be used to explore whether autocorrelations other than ρ_6 can provide additional information. Ultimately, the PPEs should be used to constrain model parameters based on observations of autocorrelations to fully probe their information content. To do this, it will be necessary to provide better uncertainty estimates than the one global value we have presented in this paper. Our study suggests that the number of observations used is a strong indicator of observational uncertainty but this effect is not yet included in our estimate.

Although we have studied satellite observations because they provide a global view, our methodology can be applied to arbitrary datasets. In particular, it could be interesting to explore surface black carbon concentrations (from e.g. ACTRIS[12]) to better understand absorbing aerosol. Our methodology can also easily be modified to explore *spatial* autocorrelations which may yet contain different information. A preliminary study suggests that over the regions studied in this paper, temporal and spatial autocorrelations behave quite differently.

Code and data availability. AERONET Direct Sun data was downloaded from `https://aeronet.gsfc.nasa.gov`. The satellite super-observations are available, upon request, from the first author. AEROCOM model data was downloaded from the AEROCOM data server, see `https://aerocom.met.no/data/download`. The Perturbed Parameter Ensembles are available, upon request, from either L. Regayre (UKESM1-A) or Y. Bhatti (ECHAM-HAM). The ESEm tool for emulation can be found at `https://doi.org/10.5281/zenodo.5466563` (Watson-Parris et al., 2021b).

Author contributions. NS performed the analyses and wrote up the paper. YB, GF, OH, AL, LR and AS provided data. EA, AL, TM and AS performed supplementary analyses. Everyone commented on the paper. The work in this paper is based on discussions that have been going on for two years between NS, EA, AA, AL, PK, TM and AS.

Competing interests. We declare no competing interests.

Acknowledgements. We thank the PI(s) and their staff for establishing and maintaining the AERONET sites used in this investigation. We are grateful to the modellers and retrieval specialists who have made their data available to us. In particular we thank the AEROCOM and AEROSAT communities who made this colation of data possible. LR was supported by the Met Office Hadley Centre Climate Programme funded by DSIT. AA, AL, PK and TM were supported by the Research Council of Finland (ACCC Flagship, grant number 359342).

[12] Aerosol, Cloud and Trace gases Research InfraStructure, `https://www.actris.eu`

https://doi.org/10.5194/egusphere-2026-2656
Preprint. Discussion started: 29 May 2026

References

Afonin, S. V., Belov, V. V., Panchenko, M. V., Sakerin, S. M., and Engel', M. V.: Correlation analysis of spatial fields of the aerosol optical thickness on the base of MODIS data, Atmos. Oceanic Opt, 21, 443, 2008.

Albrecht, B. A.: Aerosols, cloud microphysics, and fractional cloudiness, Science, 245, 1227–1230, https://doi.org/10.1126/science.245.4923.1227, 1989.

Anderson, T. E., Charlson, R. J., Winker, D. M., Ogren, J. A., and Holmen, K.: Mesoscale Variations of Tropospheric Aerosols, J. Atmospheric Sciences, 60, 119–136, 2003.

Andrews, E., Ogren, J. A., Kinne, S., and Samset, B.: Comparison of AOD, AAOD and column single scattering albedo from AERONET retrievals and in situ profiling measurements, Atmospheric Chemistry and Physics, 17, 6041–6072, https://doi.org/10.5194/acp-17-6041-2017, 2017.

Angstrom, B. A.: Atmospheric turbidity , global illumination and planetary albedo of the earth, Tellus, XIV, 435–450, 1962.

Asmi, A., Wiedensohler, A., Laj, P., Fjaeraa, A. M., Sellegri, K., Birmili, W., Weingartner, E., Baltensperger, U., Zdimal, V., Zikova, N., Putaud, J. P., Marinoni, A., Tunved, P., Hansson, H. C., Fiebig, M., Kivekäs, N., Lihavainen, H., Asmi, E., Ulevicius, V., Aalto, P. P., Swietlicki, E., Kristensson, A., Mihalopoulos, N., Kalivitis, N., Kalapov, I., Kiss, G., Leeuw, G. D., Henzing, B., Harrison, R. M., Beddows, D., O'Dowd, C., Jennings, S. G., Flentje, H., Weinhold, K., Meinhardt, F., Ries, L., and Kulmala, M.: Number size distributions and seasonality of submicron particles in Europe 2008-2009, Atmospheric Chemistry and Physics, 11, 5505–5538, https://doi.org/10.5194/acp-11-5505-2011, 2011.

Ballester, J., Burns, J. C., Cayan, D., Nakamura, Y., Uehara, R., and Rodó, X.: Kawasaki disease and ENSO-driven wind circulation, Geophysical Research Letters, 40, 2284–2289, https://doi.org/10.1002/grl.50388, 2013.

Beelen, R., Raaschou-Nielsen, O., Stafoggia, M., Andersen, Z. J., Weinmayr, G., Hoffmann, B., Wolf, K., Samoli, E., Fischer, P., Nieuwenhuijsen, M., Vineis, P., Xun, W. W., Katsouyanni, K., Dimakopoulou, K., Oudin, A., Forsberg, B., Modig, L., Havulinna, A. S., Lanki, T., Turunen, A., Oftedal, B., Nystad, W., Nafstad, P., Faire, U. D., Pedersen, N. L., Östenson, C.-G., Fratiglioni, L., Penell, J., Korek, M., Pershagen, G., Eriksen, K. T., Overvad, K., Ellermann, T., Eeftens, M., Peeters, P. H., Meliefste, K., Wang, M., de Mesquita, B. B., Sugiri, D., Krämer, U., Heinrich, J., de Hoogh, K., Key, T., Peters, A., Hampel, R., Concin, H., Nagel, G., Ineichen, A., Schaffner, E., Probst-Hensch, N., Künzli, N., Schindler, C., Schikowski, T., Adam, M., Phuleria, H., Vilier, A., Clavel-Chapelon, F., Declercq, C., Grioni, S., Krogh, V., Tsai, M.-Y., Ricceri, F., Sacerdote, C., Galassi, C., Migliore, E., Ranzi, A., Cesaroni, G., Badaloni, C., Forastiere, F., Tamayo, I., Amiano, P., Dorronsoro, M., Katsoulis, M., Trichopoulou, A., Brunekreef, B., and Hoek, G.: Effects of long-term exposure to air pollution on natural-cause mortality: an analysis of 22 European cohorts within the multicentre ESCAPE project, The Lancet, 6736, 1–11, https://doi.org/10.1016/S0140-6736(13)62158-3, 2013.

Benkovitz, C. M., Easter, R. C., Nemesure, S., Wagener, R., Schwartz, E., and Abstract, A.: Sulfate over the North Atlantic and adjacent continental regions : Evaluation for October and November 1986 using a three-dimensional model driven by observation-derived meteorology, J. Geophysical Research, 99, 20 725–20 756, 1994.

Bhatti, Y. A., Revell, L. E., Schuddeboom, A. J., McDonald, A. J., Archibald, A. T., Williams, J., Venugopal, A. U., Hardacre, C., and Behrens, E.: The sensitivity of Southern Ocean atmospheric dimethyl sulfide (DMS) to modeled oceanic DMS concentrations and emissions, Atmospheric Chemistry and Physics, 23, 15 181–15 196, https://doi.org/10.5194/acp-23-15181-2023, 2023.

https://doi.org/10.5194/egusphere-2026-2656
Preprint. Discussion started: 29 May 2026

Bhatti, Y. A., Revell, L. E., McDonald, A. J., Archibald, A. T., Schuddeboom, A. J., Williams, J., Hardacre, C., Mulcahy, J., and Lin, D.: Aerosol and Dimethyl Sulfide Sensitivity to Sulfate Chemistry Schemes, Journal of Geophysical Research: Atmospheres, 129, https://doi.org/10.1029/2023JD040635, 2024.

Bhatti, Y. A., Watson-Parris, D., Regayre, L. A., Jia, H., Neubauer, D., Im, U., Svenhag, C., Schutgens, N., Tsikerdekis, A., Nenes, A., Irfan, M., van Diedenhoven, B., Arifi, A., Fu, G., and Hasekamp, O. P.: Uncertainty in aerosol effective radiative forcing from anthropogenic and natural aerosol parameters in ECHAM6.3-HAM2.3, Atmospheric Chemistry and Physics, 26, 269–293, https://doi.org/10.5194/acp-26-269-2026, 2026.

Box, G., Jenkins, G., Reinsel, G., and Ljung, G.: Time series analysis: forecasting and control, Wiley and Sons, 5th edition edn., 2016.

Brunekreef, B. and Holgate, S. T.: Air pollution and health., Lancet, 360, 1233–42, https://doi.org/10.1016/S0140-6736(02)11274-8, 2002.

Carslaw, K. S., Regayre, L. A., Proske, U., Gettelman, A., Sexton, D. M. H., Qian, Y., Marshall, L. R., Wild, O., van Lier-Walqui, M., Oertel, A., Peatier, S., Yang, B., Johnson, J. S., Li, S., McCoy, D. T., Sanderson, B. M., Williamson, C. J., Elsaesser, G. S., Yamazaki, K., and Booth, B. B. B.: Opinion: The importance and future development of perturbed parameter ensembles in climate and atmospheric science, Atmospheric Chemistry and Physics, 26, 4651–4667, https://doi.org/10.5194/acp-26-4651-2026, 2026.

Chau, K., Franklin, M., Lee, H., Garay, M., and Kalashnikova, O.: Temporal and spatial autocorrelation as determinants of regional aod-pm2.5 model performance in the middle east, Remote Sensing, 13, https://doi.org/10.3390/rs13183790, 2021.

Colarco, P. R., Kahn, R. A., Remer, L. A., and Levy, R. C.: Impact of satellite viewing-swath width on global and regional aerosol optical thickness statistics and trends, Atmospheric Measurement Techniques, 7, 2313–2335, https://doi.org/10.5194/amt-7-2313-2014, 2014.

Dockery, D., Pope, A., Xu, X., Spengler, J., Ware, J., Fay, M., Ferris, B., and Speizer, F.: An association between air pollution and mortality in six U.S. cities, The New England Journal of Medicine, 329, 1753–1759, 1993.

Eck, T. F., Holben, B. N., Reid, J. S., Smirnov, A., O'Neill, N. T., Slutsker, I., and Kinne, S.: Wavelength dependence of the optical depth of biomass burning, urban, and desert dust aerosols, J. Geophysical Research, 104, 31 333–31 349, 1999.

Ezzati, M., Lopez, A. D., Rodgers, A., Hoorn, S. V., and Murray, C. J. L.: Selected major risk factors and global and regional burden of disease., Lancet, 360, 1347–60, https://doi.org/10.1016/S0140-6736(02)11403-6, 2002.

Giles, D. M., Sinyuk, A., Sorokin, M. G., Schafer, J. S., Smirnov, A., Slutsker, I., Eck, T. F., Holben, B. N., Lewis, J. R., Campbell, J. R., Welton, E. J., Korkin, S. V., and Lyapustin, A. I.: Advancements in the Aerosol Robotic Network (AERONET) Version 3 database – automated near-real-time quality control algorithm with improved cloud screening for Sun photometer aerosol optical depth (AOD) measurements, Atmospheric Measurement Techniques, 12, 169–209, https://doi.org/10.5194/amt-12-169-2019, 2019.

Gliß, J., Mortier, A., Schulz, M., Andrews, E., Balkanski, Y., Bauer, S. E., Benedictow, A. M., Bian, H., Checa-Garcia, R., Chin, M., Ginoux, P., Griesfeller, J. J., Heckel, A., Kipling, Z., Kirkeväg, A., Kokkola, H., Laj, P., Sager, P. L., Lund, M. T., Myhre, C. L., Matsui, H., Myhre, G., Neubauer, D., Noije, T. V., North, P., Olivié, D. J., Rémy, S., Sogacheva, L., Takemura, T., Tsigaridis, K., and Tsyro, S. G.: AeroCom phase III multi-model evaluation of the aerosol life cycle and optical properties using ground- And space-based remote sensing as well as surface in situ observations, Atmospheric Chemistry and Physics, 21, 87–128, https://doi.org/10.5194/acp-21-87-2021, 2021.

Hamilton, D. S., Lee, L. A., Pringle, K. J., Reddington, C. L., Spracklen, D. V., and Carslaw, K. S.: Occurrence of pristine aerosol environments on a polluted planet, Proceedings of the National Academy of Sciences of the United States of America, 111, 18 466–18 471, https://doi.org/10.1073/pnas.1415440111, 2014.

Hansen, J., Sato, M., and Ruedy, R.: Radiative forcing and climate response, Journal of Geophysical Research, 102, 6831–6864, 1997.

https://doi.org/10.5194/egusphere-2026-2656
Preprint. Discussion started: 29 May 2026

Holben, B. N., Eck, T. F., Slutsker, I., Tanre, D., Buis, J. P., Setzer, A., Vermote, E., Reagan, J. A., Kaufman, Y. J., Nakajima, T., Lavenu, F., Jankowiak, I., and Smirnov, A.: AERONET-A Federated Instrument Network and Data Archive for Aerosol Characterization, Remote Sensing of Environment, 66, 1–16, 1998.

Jacob, D.: Introduction to Atmospheric Chemistry, Princeton University Press, 1999.

Johnson, J. S., Regayre, L. A., Yoshioka, M., Pringle, K. J., Turnock, S. T., Browse, J., Sexton, D. M. H., Rostron, J. W., Schutgens, N. A. J., Partridge, D. G., and Liu, D.: Robust observational constraint of uncertain aerosol processes and emissions in a climate model and the effect on aerosol radiative forcing, Atmospheric Chemistry and Physics, 20, 9491–9524, 2020.

Kaku, K. C., Reid, J. S., Hand, J. L., Edgerton, E. S., Holben, B. N., Zhang, J., and Holz, R. E.: Assessing the Challenges of Surface-Level Aerosol Mass Estimates From Remote Sensing During the SEAC4RS and SEARCH Campaigns: Baseline Surface Observations and Remote Sensing in the Southeastern United States, Journal of Geophysical Research: Atmospheres, 123, 7530–7562, https://doi.org/10.1029/2017JD028074, 2018.

Kinne, S., O'Donnel, D., Stier, P., Kloster, S., Zhang, K., Schmidt, H., Rast, S., Giorgetta, M., Eck, T. F., and Stevens, B.: MAC-v1: A new global aerosol climatology for climate studies, Journal of Advances in Modeling Earth Systems, 5, 704–740, https://doi.org/10.1002/jame.20035, 2013.

Kovacs, T.: Comparing MODIS and AERONET aerosol optical depth at varying separation distances to assess ground-based validation strategies for spaceborne lidar, Journal of Geophysical Research, 111, D24 203, https://doi.org/10.1029/2006JD007349, 2006.

Labordena, M., Neubauer, D., Folini, D., Patt, A., and Lilliestam, J.: Blue skies over China : The effect of pollution- control on solar power generation and revenues, PLOSone, 13, https://doi.org/10.1371/journal.pone.0207028, 2018.

Leblanc, S. E., Segal-Rozenhaimer, M., Redemann, J., Flynn, C., Johnson, R. R., Dunagan, S. E., Dahlgren, R., Kim, J., Choi, M., Silva, A. D., Castellanos, P., Tan, Q., Ziemba, L., Thornhill, K. L., and Kacenelenbogen, M.: Airborne observations during KORUS-AQ show that aerosol optical depths are more spatially self-consistent than aerosol intensive properties, Atmospheric Chemistry and Physics, 22, 11 275–11 304, https://doi.org/10.5194/acp-22-11275-2022, 2022.

Lee, L. A., Pringle, K. J., Reddington, C. L., Mann, G. W., Stier, P., Spracklen, D. V., Pierce, J. R., and Carslaw, K. S.: The magnitude and causes of uncertainty in global model simulations of cloud condensation nuclei, Atmospheric Chemistry and Physics, 13, 8879–8914, https://doi.org/10.5194/acp-13-8879-2013, 2013.

Li, X., Wagner, F., Peng, W., Yang, J., and Mauzerall, D. L.: Reduction of solar photovoltaic resources due to air pollution in China, Proceedings of the National Academy of Sciences, 114, 11 867–11 872, https://doi.org/10.1073/pnas.1711462114, 2017.

Lohmann, U. and Feichter, J.: Impact of sulfate aerosols on albedo and lifetime of clouds : A sensitivity study with the ECHAM4 GCM, Journal of Geophysical Research, 102, 13,685–13,700, 1997.

Lohmann, U. and Feichter, J.: Global indirect aerosol effects : a review, Atmospheric Chemistry and Physics, 5, 715–737, 2005.

Maher, B., Prospero, J., Mackie, D., Gaiero, D., Hesse, P., and Balkanski, Y.: Global connections between aeolian dust, climate and ocean biogeochemistry at the present day and at the last glacial maximum, Earth-Science Reviews, 99, 61–97, https://doi.org/10.1016/j.earscirev.2009.12.001, 2010.

Masonis, S. J., Anderson, T. L., Covert, D. S., Kapustin, V., Clarke, A. D., Howell, S., and Moore, K.: A Study of the Extinction-to-Backscatter Ratio of Marine Aerosol during the Shoreline Environment Aerosol Study *, Journal of Atmospheric and Oceanic Technology, 20, 2002.

McTainsh, G. and Strong, C.: The role of aeolian dust in ecosystems, Geomorphology, 89, 39–54, https://doi.org/10.1016/j.geomorph.2006.07.028, 2007.

https://doi.org/10.5194/egusphere-2026-2656
Preprint. Discussion started: 29 May 2026

Mishra, A. K., Rudich, Y., and Koren, I.: Spatial boundaries of Aerosol Robotic Network observations over the Mediterranean basin, Geophysical Research Letters, 43, 2259–2266, https://doi.org/10.1002/2015GL067630, 2016.

Neubauer, D., Ferrachat, S., Drian, C. S.-L., Stier, P., Partridge, D. G., Tegen, I., Bey, I., Stanelle, T., Kokkola, H., and Lohmann, U.: The global aerosol-climate model ECHAM6.3-HAM2.3-Part 2: Cloud evaluation, aerosol radiative forcing, and climate sensitivity, Geoscientific Model Development, 12, 3609–3639, https://doi.org/10.5194/gmd-12-3609-2019, 2019.

Nowosad, J., Stach, A., Kasprzyk, I., Grewling, Latałowa, M., Puc, M., Myszkowska, D., Weryszko-Chmielewska, E., Piotrowska-Weryszko, K., Chłopek, K., Majkowska-Wojciechowska, B., and Uruska, A.: Temporal and spatiotemporal autocorrelation of daily concentrations of Alnus, Betula, and Corylus pollen in Poland, Aerobiologia, 31, 159–177, https://doi.org/10.1007/s10453-014-9354-2, 2015.

O'Hagan, A.: Bayesian analysis of computer code outputs: A tutorial, Reliability Engineering and System Safety, 91, 1290–1300, https://doi.org/10.1016/j.ress.2005.11.025, 2006.

Perkins, R. J., Marinescu, P. J., Levin, E. J., Collins, D. R., and Kreidenweis, S. M.: Long- and short-term temporal variability in cloud condensation nuclei spectra over a wide supersaturation range in the Southern Great Plains site, Atmospheric Chemistry and Physics, 22, 6197–6215, https://doi.org/10.5194/acp-22-6197-2022, 2022.

Press, W., B.P., F., S.A., T., and Vetterling, W.: Numerical Recipes, Cambridge University Press, 1989.

Regayre, L., Johnson, J. S., Yoshioka, M., Pringle, K. J., Sexton, D. M. H., Booth, B. B. B., Lee, L. A., Bellouin, N., and Carslaw, K. S.: Aerosol and host climate model parameters are both important sources of uncertainty in aerosol ERF, Atmospheric Chemistry and Physics, pp. 1–54, https://doi.org/10.5194/acp-2018-175, 2018.

Regayre, L. A., Deaconu, L., Grosvenor, D. P., Sexton, D. M., Symonds, C., Langton, T., Watson-Paris, D., Mulcahy, J. P., Pringle, K. J., Richardson, M., Johnson, J. S., Rostron, J. W., Gordon, H., Lister, G., Stier, P., and Carslaw, K. S.: Identifying climate model structural inconsistencies allows for tight constraint of aerosol radiative forcing, Atmospheric Chemistry and Physics, 23, 8749–8768, https://doi.org/10.5194/acp-23-8749-2023, 2023.

Regayre, L. A., Prévost, L. M. C., Ghosh, K., Johnson, J. S., Oakley, J. E., Owen, J., Webb, I., and Carslaw, K. S.: Remaining aerosol forcing uncertainty after observational constraint and the processes that cause it, Atmospheric Chemistry and Physics, 26, 2293–2317, https://doi.org/10.5194/acp-26-2293-2026, 2026.

Sayer, A. M.: How Long Is Too Long? Variogram Analysis of AERONET Data to Aid Aerosol Validation and Intercomparison Studies, Earth and Space Science, 7, https://doi.org/10.1029/2020EA001290, 2020.

Sayer, A. M., Munchak, L. A., Hsu, N. C., Levy, R. C., Bettenhausen, C., and Jeong, M. J.: Modis collection 6 aerosol products: Comparison between aqua's e-deep blue, dark target, and "merged" data sets, and usage recommendations, Journal of Geophysical Research, 119, 13,965–13,989, https://doi.org/10.1002/2014JD022453, 2014.

Schepanski, K., Klüser, L., Heinold, B., and Tegen, I.: Spatial and temporal correlation length as a measure for the stationarity of atmospheric dust aerosol distribution, Atmospheric Environment, 122, 10–21, https://doi.org/10.1016/j.atmosenv.2015.09.034, 2015.

Schmid, B., Michalsky, J., Halthore, R., Beauharnois, M., Harnson, L., Livingston, J., Russell, P., Holben, B., Eck, T., and Smirnov, A.: Comparison of Aerosol Optical Depth from Four Solar Radiometers During the Fall 1997 ARM Intensive Observation Period, Geophysical Research Letters, 26, 2725–2728, 1999.

Schutgens, N., Partridge, D. G., and Stier, P.: The importance of temporal collocation for the evaluation of aerosol models with observations, Atmospheric Chemistry and Physics, 16, 1065–1079, https://doi.org/10.5194/acp-16-1065-2016, 2016a.

Schutgens, N., Tsyro, S., Gryspeerdt, E., Goto, D., Weigum, N., Schulz, M., and Stier, P.: On the spatio-temporal representativeness of observations, Atmospheric Chemistry and Physics, 17, 9761–9780, https://doi.org/10.5194/acp-2017-149, 2017.

https://doi.org/10.5194/egusphere-2026-2656
Preprint. Discussion started: 29 May 2026

Schutgens, N., Sayer, A. M., Heckel, A., Hsu, C., Jethva, H., Leeuw, G. D., Leonard, P. J. T., Levy, R. C., Lipponen, A., Lyapustin, A., North, P., Popp, T., Poulsen, C., Sawyer, V., Sogacheva, L., Thomas, G., Torres, O., Wang, Y., Kinne, S., Schulz, M., and Stier, P.: An AeroCom – AeroSat study : intercomparison of satellite AOD datasets for aerosol model evaluation, Atmospheric Chemistry and Physics, 20, 12 431–12 457, https://doi.org/10.5194/acp-20-12431-2020, 2020.

Schutgens, N., Dubovik, O., Hasekamp, O., Torres, O., Jethva, H., Leonard, P. J. T., Litvinov, P., Redemann, J., Shinozuka, Y., de Leeuw, G., Kinne, S., Pop, T., Schulz, M., and Stier, P.: AEROCOM and AEROSAT AAOD and SSA study – Part 1 : Evaluation and intercomparison of satellite measurements, Atmospheric Chemistry and Physics, 21, 6895–6917, 2021.

Schutgens, N. A. and Stier, P.: A pathway analysis of global aerosol processes, Atmospheric Chemistry and Physics, 14, 11 657–11 686, https://doi.org/10.5194/acp-14-11657-2014, 2014.

Schutgens, N. A. J.: Site representativity of AERONET and GAW remotely sensed aerosol optical thickness and absorbing aerosol optical thickness observations, Atmospheric Chemistry and Physics, 20, 7473–7488, https://doi.org/10.5194/acp-20-7473-2020, 2020.

Schutgens, N. A. J., Gryspeerdt, E., Weigum, N., Tsyro, S., Goto, D., Schulz, M., and Stier, P.: Will a perfect model agree with perfect observations ? The impact of spatial sampling, Atmospheric Chemistry and Physics, 16, 6335–6353, https://doi.org/10.5194/acp-16-6335-2016, 2016b.

Sellar, A. A., Jones, C. G., Mulcahy, J. P., Tang, Y., Yool, A., Wiltshire, A., O'Connor, F. M., Stringer, M., Hill, R., Palmieri, J., Woodward, S., de Mora, L., Kuhlbrodt, T., Rumbold, S. T., Kelley, D. I., Ellis, R., Johnson, C. E., Walton, J., Abraham, N. L., Andrews, M. B., Andrews, T., Archibald, A. T., Berthou, S., Burke, E., Blockley, E., Carslaw, K., Dalvi, M., Edwards, J., Folberth, G. A., Gedney, N., Griffiths, P. T., Harper, A. B., Hendry, M. A., Hewitt, A. J., Johnson, B., Jones, A., Jones, C. D., Keeble, J., Liddicoat, S., Morgenstern, O., Parker, R. J., Predoi, V., Robertson, E., Siahaan, A., Smith, R. S., Swaminathan, R., Woodhouse, M. T., Zeng, G., and Zerroukat, M.: UKESM1: Description and Evaluation of the U.K. Earth System Model, Journal of Advances in Modeling Earth Systems, 11, 4513–4558, https://doi.org/10.1029/2019MS001739, 2019.

Shinozuka, Y. and Redemann, J.: Horizontal variability of aerosol optical depth observed during the ARCTAS airborne experiment, Atmospheric Chemistry and Physics, 11, 8489–8495, https://doi.org/10.5194/acp-11-8489-2011, 2011.

Smirnov, A., Holben, B. N., Eck, T. F., Dubovik, O., and Slutsker, I.: Cloud-Screening and Quality Control Algorithms for the AERONET Database, Remote Sensing of Environment, 73, 337–349, 2000.

Smith, K. R., Jerrett, M., Anderson, H. R., Burnett, R. T., Stone, V., Derwent, R., Atkinson, R. W., Cohen, A., Shonkoff, S. B., Krewski, D., Pope, C. A., Thun, M. J., and Thurston, G.: Public health benefits of strategies to reduce greenhouse-gas emissions: health implications of short-lived greenhouse pollutants., Lancet, 374, 2091–103, https://doi.org/10.1016/S0140-6736(09)61716-5, 2009.

Sullivan, R. C., Levy, R. C., Silva, A. M. D., and Pryor, S. C.: Developing and diagnosing climate change indicators of regional aerosol optical properties, Scientific Reports, 7, https://doi.org/10.1038/s41598-017-18402-x, 2017.

Swap, R., Garstang, M., Greco, S., Talbot, R., and Kallberg, P.: Saharan dust in the Amazon Basin, Tellus, 44B, 133–149, https://doi.org/10.1034/j.1600-0889.1992.t01-1-00005.x, 1992.

Targino, A., Noone, K., and Öström, E.: Airborne in situ characterization of dry aerosol optical properties in a multisource influenced marine region, Tellus-B, 57, 247–260, 2005.

Tegen, I., Neubauer, D., Ferrachat, S., le Drian, C. S., Bey, I., Schutgens, N., Stier, P., Watson-parris, D., Stanelle, T., Schmidt, H., and Rast, S.: The global aerosol – climate model ECHAM6 . 3 – HAM2 . 3 – Part 1 : Aerosol evaluation, Geoscientific Model Development, 3, 1643–1677, 2019.

https://doi.org/10.5194/egusphere-2026-2656
Preprint. Discussion started: 29 May 2026

Textor, C., Schulz, M., Guibert, S., Kinne, S., Balkanski, Y., Bauer, S., Berntsen, T., Berglen, T., Boucher, O., Chin, M., Dentener, F., Diehl, T., Feichter, J., Fillmore, D., Ginoux, P., Gong, S., Grini, A., Hendricks, J., Horowitz, L., Huang, P., a. Isaksen, I. S., Iversen, T., Kloster, S., Koch, D., Kirkevåg, A., Kristjansson, J. E., Krol, M., Lauer, A., Lamarque, J. F., Liu, X., Montanaro, V., Myhre, G., Penner, J. E., Pitari, G., Reddy, M. S., Seland, O., Stier, P., Takemura, T., and Tie, X.: The effect of harmonized emissions on aerosol properties in global models – an AeroCom experiment, Atmospheric Chemistry and Physics, 7, 4489–4501, https://doi.org/10.5194/acp-7-4489-2007, 2007.

Twomey, S.: Pollution and the planetary albedo, Atmospheric Environment, 8, 1251–1256, 1974.

Vink, S. and Measures, C.: The role of dust deposition in determining surface water distributions of Al and Fe in the South West Atlantic, Deep Sea Research Part II, 48, 2787–2809, https://doi.org/10.1016/S0967-0645(01)00018-2, 2001.

Watson-Parris, D., Williams, A., Deaconu, L., and Stier, P.: Model calibration using ESEm v1.1.0-an open, scalable Earth system emulator, Geoscientific Model Development, 14, 7659–7672, https://doi.org/10.5194/gmd-14-7659-2021, 2021a.

Watson-Parris, D., Williams, A., Deaconu, L., and Stier, P.: duncanwp/ESEm: v1.1.0, Zenodo [software], https://doi.org/10.5281/zenodo.5466563, 2021b.

Wehner, B. and Wiedensohler, A.: Atmospheric Chemistry and Physics Long term measurements of submicrometer urban aerosols: statistical analysis for correlations with meteorological conditions and trace gases, Atmos. Chem. Phys, 3, 867–879, www.atmos-chem-phys.org/acp/3/867/, 2003.

Weigum, N. M., Stier, P., Schwarz, J. P., Fahey, D. W., and Spackman, J. R.: Scales of variability of black carbon plumes over the Pacific Ocean, Geophysical Research Letters, 39, https://doi.org/10.1029/2012GL052127, 2012.

Yoshioka, M., Regayre, L. A., Pringle, K. J., Johnson, J. S., Mann, G. W., Partridge, D. G., Sexton, D. M., Lister, G. M., Schutgens, N., Stier, P., Kipling, Z., Bellouin, N., Browse, J., Booth, B. B., Johnson, C. E., Johnson, B., Mollard, J. D., Lee, L., and Carslaw, K. S.: Ensembles of Global Climate Model Variants Designed for the Quantification and Constraint of Uncertainty in Aerosols and Their Radiative Forcing, Journal of Advances in Modeling Earth Systems, 11, 3728–3754, https://doi.org/10.1029/2019MS001628, 2019.

Zhong, Q., Schutgens, N., Werf, G. R. V. D., Noije, T. V., Bauer, S. E., Tsigaridis, K., Mielonen, T., Checa-garcia, R., Neubauer, D., Kipling, Z., Kirkevåg, A., Olivié, D. J. L., Kokkola, H., Matsui, H., Ginoux, P., Takemura, T., Sager, P. L., Rémy, S., Bian, H., and Chin, M.: Using modelled relationships and satellite observations to attribute modelled aerosol biases over biomass burning regions, Nature Communications, https://doi.org/10.1038/s41467-022-33680-4, 2022.

Zhong, Q., Schutgens, N., Werf, G. R. V. D., Takemura, T., Noije, T. V., Mielonen, T., Checa-Garcia, R., Lohmann, U., Kirkevåg, A., Olivié, D. J. L., Kokkola, H., Matsui, H., Kipling, Z., Ginoux, P., Sager, P. L., Rémy, S., Bian, H., Chin, M., Zhang, K., Bauer, S. E., and Tsigaridis, K.: Threefold reduction of modeled uncertainty in direct radiative effects over biomass burning regions by constraining absorbing aerosols, Science Advances, 9, https://www.science.org, 2023.

Émeline Lequy, Conil, S., and Turpault, M.-P.: Impacts of Aeolian dust deposition on European forest sustainability: A review, Forest Ecology and Management, 267, 240–252, https://doi.org/10.1016/j.foreco.2011.12.005, 2012.